

1 **Archaeal community composition in Holocene methane pockmarks of the Gdańsk Basin**
2 **(Baltic Sea, Poland): insights from tetraether lipids and 16S rRNA analysis**

3
4 Izabela De Mey-Śnieżyńska^{1*}, Mirosław Słowakiewicz¹, Francien Peterse², Aleksandra
5 Brodecka-Goluch⁴, Andrzej Borkowski³, Katarzyna Łukawska-Matuszewska⁴

6
7 ¹University of Warsaw, Faculty of Geology, 02-089 Warsaw, Poland

8 ²Utrecht University, Department of Earth Sciences, 3584 CS Utrecht, The Netherlands

9 ³AGH University of Krakow, Faculty of Geology, Geophysics and Environmental Protection, 30-059
10 Kraków, Poland

11 ⁴University of Gdańsk, Faculty of Oceanography and Geography, 81-379 Gdynia, Poland

12
13 *Corresponding author: i.sniezynska@uw.edu.pl

14
15
16 **Highlights**

17 Pockmark sediments harbour substantially higher archaeal diversity and abundance than non-
18 pockmark reference sediments.

19 The P/MET4 pockmark in the Gdańsk Deep hosts the most diverse and abundant methanogen
20 community, coinciding with the highest concentrations of isoprenoid glycerol dialkyl glycerol
21 tetraether lipids (iGDGTs).

22 Crenarchaeol dominates the iGDGT pool in both pockmark and reference sediment cores,
23 indicating strong Nitrososphaeria-related iGDGT synthesis in the water column.

24 **Abstract**

25 Methane pockmarks and shallow gas systems are prominent geomorphological features in the
26 Baltic Sea that act as hotspots of microbial activity. In the Gdańsk Basin, pockmarks vary in
27 gas-seepage intensity and in the extent of freshened porewater discharge, both of which
28 influence the archaeal community structure and the composition of internal methane biofilters.
29 The objective of this study was to examine the effects of methane seepage and freshened
30 porewater on the composition of archaeal communities and on the isoprenoid glycerol dialkyl

31 glycerol tetraethers (iGDGTs), membrane lipids synthesised by these communities, across the
32 gas systems examined. Additionally, the effects of these environmental factors on the use and
33 interpretation of iGDGT-based proxies under conditions of gas and water seepage were
34 assessed. The study investigates whether iGDGT patterns in these Baltic gas systems reflect
35 methane-driven processes, including anaerobic oxidation of methane (AOM) and
36 methanogenesis, porewater freshening, or pelagic contributions from ammonia-oxidising
37 archaea (AOA). The results show elevated iGDGT concentrations in pockmark cores compared
38 with reference non-pockmark cores; however, the summed iGDGT concentration varies by site.
39 Overall, iGDGT concentrations are much higher at sites with reduced seabed pockmark activity
40 and weak porewater freshening. Nevertheless, consistently low Methane Index values ($MI <$
41 0.09), together with low GDGT-0/crenarchaeol (< 1) and low GDGT-2/cren (< 0.04) ratios,
42 indicate that the iGDGT pool lacks the typical enrichment in GDGT-1 to -3 associated with
43 AOM, suggesting no AOM imprint on the iGDGT pool. However, 16S rRNA analysis revealed
44 that the anaerobic methanotrophic archaeal lineages (ANME) consist of ANME-2b and ANME-
45 3. A strong positive correlation between OH-GDGTs and crenarchaeol, together with the
46 consistency of OH-GDGT% values with those previously reported for Baltic Sea surface
47 sediments, suggests a thaumarchaeal source of iGDGTs in the studied pockmark and reference
48 cores. The Branched and Isoprenoid Tetraether (BIT) index values suggest marine archaeal
49 GDGT production. In this system, iGDGT-based proxies primarily reflect a strong pelagic
50 presence of AOA, as indicated by the dominance of crenarchaeol. This suggests that, despite
51 the local presence of methanogenic and ANME-related archaeal groups, methane-related AOM
52 does not influence the iGDGT signal due to the archaeal community structure. These findings
53 highlight the complex interplay between freshened porewater and gas seepage in shaping
54 archaeal communities, and the role of ammonia-oxidising Nitrososphaeria in controlling
55 iGDGT composition and the sedimentary record.

56 **Keywords:** methane, pockmarks, iGDGTs, ammonia-oxidising archaea, crenarchaeol,
57 Holocene, Gdańsk Deep, Baltic Sea

58

59 **1 Introduction**

60 Pockmarks are concave geological structures ranging from a few meters up to several hundred
61 meters in width and up to 100 meters in depth, formed by gas and/or water seepage from the
62 sediments into the hydrosphere (King and MacLean, 1970; Hovland and Judd, 1988). As

63 indicators of hydraulic activity, they are categorised as active or inactive depending on whether
64 gas and/or water seepage is continuous or dormant/intermittent (Hovland and Judd, 1988;
65 Hovland et al., 2002). Their morphology facilitate detection through geophysical and
66 hydroacoustic surveys, making pockmarks practical proxies for investigating seepage
67 phenomena (Hovland and Judd, 1988), which occur globally on continental shelves and margins,
68 including off Nova Scotia (King and MacLean, 1970), thousands of newly discovered
69 pockmarks offshore California (Lundsten et al., 2024), in the Gulf of Mexico (Roberts and
70 Aharon, 1994; Lawal et al., 2026). The formation of pockmarks requires pressure buildup in
71 fine-grained, low-permeability sediments, with methane (CH₄) as the most commonly emitted
72 component because of its high mobility (Hovland and Judd, 1988). Seepage types vary globally
73 and include biogenic, thermogenic, or hydrothermal gas seepage; groundwater; or combined
74 gas-and-water seepage (Hovland and Judd, 1988). Pockmarks predominantly form along salt-
75 dome margins (Schmuck and Paull, 1993; Taylor et al., 2000) and in dislocation zones, faults,
76 and bedrock fractures (Shaw et al., 1997). They also occur in regions of low seismicity, such as
77 Sweden (Hovland et al., 2002) and the southern Baltic Sea (Idczak et al., 2020). Glacial and
78 post-glacial processes can influence their formation by generating overpressure, as observed in
79 the North Sea (Callow et al., 2021) and the Baltic Sea (Whiticar and Werner, 1981; Whiticar,
80 2002; Kreuzburg et al., 2023). Baltic Sea pockmarks have been documented in Eckernförde
81 Bay and the Mecklenburg Bight (Werner, 1978; Wever et al., 1998; Jensen et al., 2002; Schlüter
82 et al., 2004; Hoffmann et al., 2020; Díaz-Mendoza et al., 2023), the Stockholm Archipelago
83 (Jakobsson et al., 2020), offshore Finland (Virtasalo et al., 2019), and the Gdańsk Basin
84 (Pimenov et al., 2010; Majewski and Klusek, 2011; Brodecka et al., 2013; Jaśniewicz et al.,
85 2019; Idczak et al., 2020; Brodecka-Goluch et al., 2022). The Gdańsk Basin is the focus of this
86 study.

87 In several Baltic settings, pockmarks have been linked to submarine groundwater discharge
88 (SGD), broadly defined as the movement of fresh, brackish, or saline groundwater into the sea
89 or ocean across the sediment-water interface. SGD encompasses both the inflow of freshened
90 groundwater and the recirculation of saline porewater or seawater, driven by hydraulic pressure
91 and density differences (Burnett et al., 2003, 2006; Moore, 2010; Taniguchi et al., 2019).
92 Evidence of an association between pockmarks and upward groundwater infiltration has been
93 documented in areas such as Eckernförde Bay (Bussmann and Suess, 1998; Schlüter et al.,
94 2004), Hanko Bay (Virtasalo et al., 2019; Purkamo et al., 2022), and the central Gulf of Gdańsk
95 (Szymczycha et al., 2016; Idczak et al., 2020). In the Gdańsk Basin area (Fig. 1), deep-water,

96 fine-grained pockmarks are associated with localised porewater freshening, indicated by
97 chloride (Cl^-) and sulphate (SO_4^{2-}) depletion, linked to seepage of freshened groundwater or
98 discharge of freshened porewater (Szymczycha et al., 2018; Idczak et al., 2020; Brodecka-
99 Goluch et al., 2022; Kurowski et al., 2024; Łukawska-Matuszewska and Dwornik, 2025;
100 Łukawska-Matuszewska et al., 2025). The impact of SGD discharge on pockmark sediments
101 depends on the source, chemical composition, and flow regime of the discharging fluids.
102 Nevertheless, freshened SGD and associated porewater transport can alter the distribution of
103 dissolved species, including NH_4^+ , CH_4 , dissolved inorganic carbon (DIC), H_2S , Cl^- , and SO_4^{2-}
104 , thereby shifting redox transition zones and influencing CH_4 cycling (Schlüter et al., 2004; Liu
105 et al., 2017; Idczak et al., 2020; O'Reilly et al., 2021; Brodecka-Goluch et al., 2022; Zhang et
106 al., 2025). In the pockmarks of Gdańsk Basin, Cl^- and SO_4^{2-} depletion linked to freshened
107 porewater discharge may weaken SO_4^{2-} -driven anaerobic methane oxidation (S-AOM),
108 promote shallow methanogenesis, and contribute to episodic gas release into the water column
109 (Idczak et al., 2020).

110

111 At the sulphate-methane interface (SMI), where the seafloor intersection of downward-
112 diffusing sulphate and upward-diffusing CH_4 occurs, ascending CH_4 is consumed in AOM
113 (Zehnder and Brock, 1980; Boetius et al., 2000). It is mediated by sulphate-reducing bacteria
114 (SRB) and anaerobic methanotrophic archaea (ANME) (Knittel and Boetius, 2009), which limit
115 CH_4 emissions to the water column (Reeburgh, 2007). In the Baltic Sea, a halocline at 60-80 m
116 separates oxygenated and anoxic waters, structuring key biogeochemical cycles (Kuliński et al.,
117 2022), including an oxic-suboxic nitrogen-cycling zone driven by ammonia-oxidising archaea
118 (AOA) (Berg et al., 2015b; Jäntti et al., 2018). Archaeal biomarkers for methane cycling
119 (ANME, methanogens) and nitrification (AOA), such as intact polar GDGTs (IPL-GDGTs),
120 can be transported and preserved as core isoprenoidal GDGTs (CL-iGDGTs) in sediments
121 (Schouten et al., 2013).

122

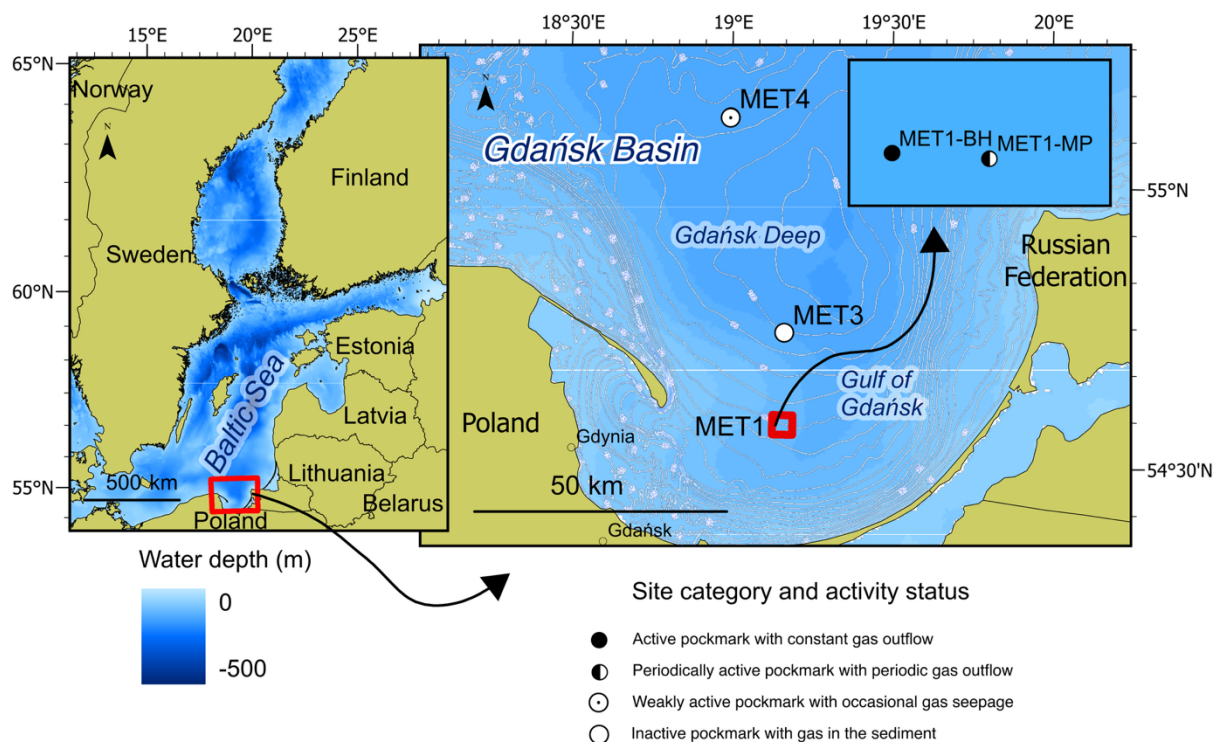
123 Archaeal iGDGTs are membrane lipids whose structures adapt to environmental changes (De
124 Rosa et al., 1977; Huguet et al., 2006; Liu et al., 2017; Schouten et al., 2002, 2013; Sinninghe
125 Damsté et al., 2022). In marine sediments, GDGT-0 and crenarchaeol dominate. Crenarchaeol
126 is produced by Thaumarchaeota (Sinninghe Damsté et al., 2002) – in current nomenclature,
127 Nitrososphaeria, class of Thermoproteota phylum (Rinke et al., 2021). Nitrososphaeria are the
128 main ammonia oxidisers (Berg et al., 2015a, b) and iGDGT synthesisers in the Baltic Sea
129 (Labrenz et al., 2010; Wittenborn et al., 2023). Methanogens primarily produce GDGT-0,

130 whereas methanotrophs, mainly ANME-1, produce GDGT-1 to -3 (Koga et al., 1993; Pancost
131 et al., 2001; Weijers et al., 2006; Rossel et al., 2008; Blaga et al., 2009; Zhang et al., 2011;
132 Inglis et al., 2015; Słowakiewicz et al., 2016; Petrick et al., 2019). Hydroxylated-GDGTs (OH-
133 GDGTs) are produced primarily by Thaumarchaeota (Sinninghe Damsté et al., 2002; Liu et al.,
134 2012; Kaiser and Arz, 2016; Elling et al., 2017; Bale et al., 2019; Sinninghe Damsté et al.,
135 2022), but can also be biosynthesised by methanogens or ANME (Liu et al., 2012; Guan et al.,
136 2024; Fenies et al., 2026). OH-GDGT synthesis reflects cold adaptation (Liu et al., 2012) and
137 salinity changes (Sinninghe Damsté et al., 2022); OH-GDGT-0 is most abundant at high
138 latitudes (Huguet et al., 2013; Varma et al., 2024) and in Baltic Sea sediments, where culture
139 studies have confirmed an AOA source (Blainey et al., 2011; Berg et al., 2015a).

140

141 Groundwater-seawater mixing zones in permeable coastal aquifers are commonly
142 conceptualised as subterranean estuaries (Moore, 1999; Ruiz-González et al., 2021). This
143 conceptual framework is useful for SGD-affected systems because microbial activity within
144 these mixing zones can modify the chemical composition of groundwater before it reaches the
145 seabed (Ruiz-González et al., 2021). Importantly, deeper groundwater mixing zones have been
146 reported to host distinct archaeal communities, including AOA populations (Santoro et al.,
147 2008; Rogers and Casciotti, 2010; Purkamo et al., 2022; Wilson et al., 2024). Therefore, in
148 addition to pelagic and sedimentary sources, groundwater-associated archaeal communities
149 should be considered as a potential source of archaeal tetraether lipids in SGD-influenced
150 marine sediments. This is particularly relevant for Baltic Sea pockmarks, where iGDGTs may
151 reflect several partly overlapping sources and processes. In the Baltic Sea water column,
152 iGDGTs and OH-GDGTs are mainly associated with Nitrososphaeria, especially *Ca.*
153 *Nitrosopumilus*, inhabiting the pelagic redoxcline (Sinninghe Damsté et al., 2022; Wittenborn
154 et al., 2023). However, GDGT-0 can also be produced by methanogenic archaea, which are
155 expected to contribute to CH₄ production in the studied pockmark sediments. Moreover,
156 although direct studies of GDGTs in SGD-affected marine sediments remain scarce,
157 groundwater studies show that both CL-iGDGTs and IPL-iGDGTs can be produced in situ by
158 indigenous subsurface microbial communities, with distributions linked to groundwater
159 thaumarchaeotal groups rather than solely to allochthonous surface inputs (Ding et al., 2018).
160 Consequently, in methane pockmark sediments affected by porewater freshening, archaeal 16S
161 rRNA and CL-iGDGT distributions may record multiple controls: the regional input of Baltic
162 pelagic AOA, sedimentary CH₄-driven processes including methanogenesis and
163 methanotrophy, and a hydrogeochemical imprint associated with freshened porewater or SGD-

164 related seawater-groundwater mixing. Because OH-GDGT distributions are also sensitive to
 165 salinity changes (Sinninghe Damsté et al., 2022), these compounds may be responsive to
 166 porewater freshening in the examined pockmarks. Thus, the studied system provides a natural
 167 setting to test whether archaeal tetraether lipids primarily reflect pelagic marine production,
 168 sedimentary methane cycling, or additional influence from freshened porewater.



169 Fig. 1. Map of the study area in the south-eastern Baltic Sea, the Gdańsk Basin. The main panel shows
 170 the Gdańsk Basin, including the Gdańsk Deep and the Gulf of Gdańsk. Symbols indicate the category
 171 and activity status of the investigated pockmark sites (tagged with a “P” prefix) with respect to venting
 172 status, based on MBES and SBES observations collected during the present and previous research
 173 campaigns in 2019-2025. Reference stations (labelled as surrounding stations and tagged with an “S”
 174 prefix) are referred to as non-pockmark cores or reference cores. They are positioned approximately
 175 100-150 m from the corresponding pockmark margins on morphologically regular seafloor lacking
 176 pockmark depressions; they are not shown separately on the map due to the map’s scale. Additional
 177 data, including CH₄/SO₄²⁻ profiles and Cl⁻ profiles, are presented in Figures 2 and 3, respectively. More
 178 detailed data, for example, concerning porewater freshening, are available in the supplementary material
 179 (Table S1). Map source: Eurostat/GISCO, 2024, scale 1.

181
 182 **2 Materials and methods**

183 **2.1 Study area**

184

185 Pockmarks in the Gdańsk Deep and the central Gulf of Gdańsk (Fig. 1) occur at water depths
186 of 1-100 m and are characterised by active gas seepage from Holocene silts and clays (Idczak
187 et al., 2020). Although the gas is predominantly biogenic (Brodecka-Goluch et al., 2022), the
188 presence of helium (up to 0.39%) (Idczak et al., 2020) and noble gases (Ne, Ar, Kr, Xe)
189 (Brodecka-Goluch et al., 2022) in samples from station MET1 suggests that these pockmarks
190 vent Middle Cambrian reservoirs, with gas migrating through sedimentary layers along faults
191 (Jaworowski et al., 2010; Idczak et al., 2020; Brodecka-Goluch et al., 2022), possibly with
192 additional contributions from the crust and mantle (Kotarba, 2010; Pokorski, 2010; Kotarba and
193 Lewan, 2013; Kotarba and Nagao, 2015).

194
195 The study area spans the Gdańsk Basin and includes stations MET3 and MET4 in the northern
196 Gdańsk Deep, and MET1-MP and MET1-BH in the Gulf of Gdańsk (Fig. 1). The southern
197 stations (MET1 area) receive a high input of terrestrial organic matter from the Vistula River,
198 trap plant material and organic debris, and experience moderate anthropogenic contamination,
199 resulting in elevated total organic carbon (TOC) (Idczak et al., 2020; Brodecka-Goluch et al.,
200 2022; Łukawska-Matuszewska et al., 2022; Szymczak-Żyła and Lubecki, 2022). Sedimentation
201 rates are lower in MET3 and MET4 ($\sim 0.17\text{--}0.20\text{ cm yr}^{-1}$) than at MET1 ($\sim 0.15\text{--}0.22\text{ cm yr}^{-1}$)
202 (Szczepańska and Uścińowicz, 1994; Brodecka-Goluch et al., 2022). In a previous study of
203 pockmarks in the Gdańsk Deep, Brodecka-Goluch et al. (2022) reported that CH₄ at pockmark
204 P/MET3 has isotopic signatures of marine microbial gas, whereas gas venting from MET1-MP
205 shows mixed marine and terrestrial signatures, indicating the upward infiltration of freshwater.
206 Thus, methanogenic pathways vary between sites: acetoclastic at MET1-BH, hydrogenotrophic
207 at MET3, and mixed at MET1-MP (Idczak et al., 2020; Brodecka-Goluch et al., 2022). The
208 MET1 pockmarks are characterised by intensive/periodic gas and freshwater seepage (Idczak
209 et al., 2020; Brodecka-Goluch et al., 2022). MET4 represents the least-studied system, located
210 within a field of multiple pockmarks (Brodecka-Goluch et al., 2020).

211
212 In the Gdańsk Basin, SGD is divided into shallow/coastal and deep/offshore components. The
213 shallow/coastal component occurs in nearshore areas and is fed by Quaternary-Cretaceous
214 coastal aquifers (e.g., Piekarek-Jankowska, 1996; Szymczycha et al., 2016, 2018). By contrast,
215 the deep/offshore component comprises artesian-type freshwater seepage with episodic
216 discharge at deep-water pockmarks such as MET1 (Szymczycha et al., 2018; Idczak et al.,
217 2020). Deep SGD originates from extensive Upper Cretaceous aquifers beneath the Gulf of
218 Gdańsk (Uścińowicz, 2011). Seepage intensity varies with hydrostatic pressure, water-column

219 processes, and fault activity (Brodecka-Goluch et al., 2022). After commercial extraction
220 ceased in 2000, natural hydrodynamic conditions returned (Uścińowicz, 2011), although the
221 extent and periodicity of deep discharge remain unquantified. SGD in the MET1 area reduces
222 sulphate and chloride concentrations with depth, thereby compressing the SMI to a few cm
223 below the seafloor (Idczak et al., 2020; Brodecka-Goluch et al., 2022; Łukawska-Matuszewska
224 and Dwornik, 2025). A high carbonate alkalinity flux at MET1-MP indicates substantial DIC
225 generation during anaerobic diagenesis, potentially linked to Fe(III)-AOM (Łukawska-
226 Matuszewska and Dwornik, 2025). The near-bottom chloride concentration in the Gulf of
227 Gdańsk ranges from 150 to 180 mmol L⁻¹, equivalent to ~5318-6384 mg dm⁻³ (Lukawska-
228 Matuszewska, 2016). For the Gdańsk Deep, the mean value is approximately 12 PSU,
229 equivalent to 6700-6900 mg dm⁻³ (Kapustina et al., 2026).

230

231 **2.2 Sampling at MET stations**

232

233 The research stations were divided into pockmarks (morphologically concave geological
234 structures with gas emissions to the water column and/or gas-bearing sediments with possible
235 SGD) and references (non-pockmark reference sites with gas in the sediments but without
236 emission to the water column or SGD). Pockmark stations were further classified (see
237 supplementary material Table S1) based on previous studies, including hydroacoustic and
238 geophysical investigations (Brodecka-Goluch et al., 2020, 2022; Idczak et al., 2020), as well as
239 data included in this study (SO₄²⁻ and CH₄ profiles: Fig. 2; Cl⁻ profiles: Fig. 2; echograms for
240 pockmarks P/MET3 and P/MET4: supplementary material Fig. S1), as active (gas emission to
241 the water column, influence of freshened porewater, or both: P/MET1-BH, P/MET1-MP),
242 weakly active (gas seepage and porewater freshening: P/MET4), or inactive (gas present in the
243 sediments without clear emission or freshwater seepage: P/MET3).

244

245 Eight 95 cm-long sediment cores were collected from the central parts of methane-seeping
246 structures in the central Gdańsk Basin (south-eastern Baltic Sea) using a gravity corer at three
247 areas and four study locations (MET1: MET1-MP, MET1-BH; MET3; MET4; Fig. 1,
248 supplementary material Table S1) during a cruise aboard RV *Oceanograf* (University of
249 Gdańsk) in October 2019. Four additional cores were collected from outside the pockmarks
250 (~100-150 m away) as reference samples. Samples were categorised by origin: a 'P' prefix
251 (P/METX; X = 1-MP, 1-BH, 3, 4) for pockmark sediments and an 'S' prefix (S/METX) for
252 surrounding sediments, namely reference non-pockmark sediments.

253

254 Onboard, the 95 cm cores for biomarker analysis were sectioned into a top 0-5 cm interval and
255 subsequent 10 cm intervals (hereafter referred to as horizons) for the remainder of the cores,
256 yielding 72 samples for geochemical analysis (some bottom samples are missing). Samples for
257 microbial analysis were subsampled at a slightly coarser 10-cm resolution from the top (1),
258 mid-depth (5), and bottom (7, 10) intervals using a sterile spatula.

259

260 **2.3 Porewater sampling**

261

262 Porewater samples were collected under anoxic conditions from intact, hermetically sealed
263 sediment cores using Rhizon® samplers. Sediment subsamples for CH₄ determination were
264 collected immediately after core retrieval. Sampling was performed through pre-drilled holes
265 in the core liners using 3 mL syringes (with the Luer tip removed), and the material was
266 immediately transferred into 20 mL vials in accordance with the protocol described by
267 Jørgensen et al. (2001). Chloride and SO₄²⁻ concentrations in porewater were measured by high-
268 performance ion chromatography (Metrohm 850 Professional IC) with analytical precision
269 better than 3%. Methane concentrations were determined by the standard headspace technique
270 using a gas chromatograph (Perkin-Elmer) equipped with a flame ionisation detector (FID) and
271 an HP-5 capillary column (30 m × 0.32 mm × 0.25 μm), with helium as the carrier gas. The
272 method detection limit (LOD) was 0.2 μmol dm⁻³. Measured CH₄ concentrations were corrected
273 for sediment porosity. Porosity for each sample was calculated from water and organic matter
274 contents (LOI; see below) using the equations of Engvall (1978) and Carman and Jonsson
275 (1991).

276

277 **2.4 LOI analysis**

278

279 The organic matter content was assessed by gravimetric loss-on-ignition (LOI) after
280 dehydration (105° C for 24 h) and dry combustion (550° C for 6 h). Łukawska-Matuszewska et
281 al. (2014) previously demonstrated the applicability of LOI in the Gdańsk Basin as a proxy for
282 sedimentary organic matter content. LOI-based values were additionally evaluated against
283 directly measured TOC for two pockmark and reference representative cores. TOC content in
284 sediments was measured using a CHNS autoanalyser (Perkin Elmer 2400) following Parsons
285 et al. (1984). For TOC analysis, samples were acidified with 1 M HCl to remove inorganic
286 carbon, following Hedges and Stern (1984).

287

288 **2.5 Tetraether lipid extraction and analysis**

289 All freeze-dried samples were ground with a mortar and pestle. Approximately 1 g of each
290 sample was extracted with dichloromethane:methanol (DCM:MeOH, 2:1, v/v) in an ultrasonic
291 water bath. Total lipid extracts (TLEs) were chromatographed on a silica gel column with *n*-
292 hexane and methanol as eluents to obtain apolar and polar fractions, respectively.

293 The polar fraction containing core GDGTs was re-dissolved in hexane/isopropanol (99:1, v/v),
294 spiked with a known amount of an internal standard (a C₄₆ glycerol trialkyl glycerol tetraether;
295 Huguet et al., 2006), and filtered through a 0.45 µm polytetrafluoroethylene syringe filter.
296 GDGTs were analysed at Utrecht University using an ultra-high-performance liquid
297 chromatograph (UHPLC; Agilent 1260 Infinity) coupled to an Agilent 6130 single-quadrupole
298 mass detector, following the method proposed by Hopmans et al. (2016). Quantification was
299 performed by manually integrating the peak areas of the protonated ions ([M+H]⁺) in
300 ChemStation software (B.04.03), and the results were compared with those of the internal
301 standard. Selected ion monitoring (SIM) was used to detect and identify GDGTs. The target
302 ions were *m/z* 1302, 1300, 1298, 1296 and 1292 for iGDGTs and OH-GDGTs.

303 Absolute GDGT concentrations were calculated relative to the C₄₆ internal standard and
304 sediment dry weight, following established GDGT quantification approaches (Huguet et al.,
305 2006, 2010), and are therefore reported as semi-quantitative concentrations (Bijl et al., 2025).
306 Derived fractional abundances and GDGT-based indices were calculated from the integrated
307 peak areas. Raw peak areas, derived fractional abundances and indices, and semi-quantitative
308 absolute concentrations are reported in accordance with the GDGT data-reporting
309 recommendations of Bijl et al. (2025).

310 Each sediment horizon was analysed once. Replicate analyses were not available for individual
311 horizons. Therefore, sample-specific analytical uncertainty could not be estimated, and error
312 bars are not shown in the downcore plots. Method uncertainty includes peak integration,
313 instrumental response, extraction/processing effects, and the semi-quantitative nature of C₄₆-
314 based concentration estimates (Bijl et al., 2025).

315 **2.6 DNA isolation, sequencing, and data analysis**

316 Genomic DNA from the sediment samples was isolated using the EURx kit for complex
317 matrices (Soil DNA Purification Kit, no. E3570, EURX Ltd., Poland). The protocol requires
318 mechanical homogenisation to release cells from the sediment matrix. The isolated genomic
319 DNA was subjected to metabarcoding analysis. Sequencing of the hypervariable V3–V4 region
320 of the 16S rRNA gene was outsourced to GENOMED S.A. (Warsaw, Poland). Specific primer
321 sequences (developed by Zymo Research, CA, USA) were used to amplify the selected region
322 and prepare libraries (341F: CCTACGGGDGGCWGCAG, CCTAYGGGGYGWCWGCAG;
323 806R: GACTACNVGGGTMTCTAATCC).

324 PCR was performed using Q5 Hot Start High-Fidelity 2× Master Mix, with reaction conditions
325 in accordance with the manufacturer’s recommendations. Sequencing was performed on a
326 MiSeq sequencer using paired-end (PE) technology (2 × 300 nt) with Illumina’s v3 kit. FASTQ
327 files were processed with *fastp* (v. 0.23.2) (Chen et al., 2018) to improve raw sequence quality
328 by trimming adapters, filtering low-quality reads, and removing artefacts. The sequences were
329 further analysed using Kraken2 (Wood et al., 2019) following the protocol described by Lu et
330 al. (2022). The SILVA database (v. 138) was used for taxonomic assignment (Quast et al.,
331 2013). Bracken was then applied to the Kraken2 reports, set to the genus level with a threshold
332 of five (Lu et al., 2017). The resulting data were transformed before analysis. To address zero
333 values, the data were imputed using the R package *Compositions* (v. 1.4.0.1) (Palarea-
334 Albaladejo and Martín-Fernández, 2015). The centred log-ratio (clr) transformation was then
335 applied using the *Compositions* package for R (v. 2.05; Aitchison, 1982; Quinn et al., 2019; van
336 den Boogaart et al., 2024).

337 Taxonomic names are reported according to the database classification used in the
338 bioinformatic workflow. The Deep Sea Euryarchaeotic Group (DSEG) is therefore retained
339 when returned by the database, although this lineage is classified within Thermoplasmatota in
340 newer phylogenetic classifications (Rinke et al., 2021).

341

342 **2.7 Statistical analysis and data visualisation**

343 Multidimensional analyses, correlograms, and hierarchical analyses were conducted using R (R
344 Core Team, 2023). RStudio 2025.05.0+496 “Mariposa Orchid” and R version 4.3.3 (2024-02-
345 29) on the x86_64-apple-darwin20 (64-bit) platform were used for all analyses. A heatmap of
346 the archaeal community (at the class level) with cluster analysis was generated using the
347 Heatmap function in the *ComplexHeatmap* package. To examine the grouping of samples

348 between pockmark and reference sites, Classical Multidimensional Scaling (MDS; principal
349 coordinates analysis) was performed using the `dist` function (`dist_matrix <- dist(data), method`
350 `= "euclidean")` and the `cmdscale` function (`mds <- cmdscale(dist_matrix))` from the *stats*
351 package. The MDS results were visualised using the *ggplot2* and *ggrepel* packages (Wickham,
352 2016).

353 Permutational Multivariate Analysis of Variance (PERMANOVA) was conducted using
354 `adonis2` (`permutations = 999, method = "bray")` in the *vegan* package. Principal Component
355 Analysis (PCA) was conducted using the *FactoMineR* package, and the results were visualised
356 with `fviz_pca_var` from the *factoextra* package. A correlation network illustrating relationships
357 between Archaea (at the family taxonomic level) and GDGTs was constructed using `cor` from
358 the *stats* package; `graph_from_adjacency_matrix` (`mode = "undirected", weighted = TRUE,`
359 `diag = FALSE)` from the *igraph* package; `mutate_as_tbl` from the *tidygraph* package; and
360 *ggraph* for visualisation. Community structure was identified using `group_louvain` (multilevel
361 optimisation of modularity via `igraph::cluster_louvain()`), which implements the multi-level
362 modularity optimisation algorithm described by Blondel et al. (2008). Cross-correlations
363 between iGDGT and OH-GDGT concentrations were calculated in R using `stats::cor.test()` with
364 Pearson correlation. Concentrations were \log_{10} -transformed ($\log_{10}[x + 10^{-6}]$) before correlation
365 analysis to reduce right skew. Correlations were computed using pairwise complete
366 observations. To correct for multiple testing, *p*-values were adjusted using the Benjamini–
367 Hochberg false discovery rate (FDR) procedure.

368 **2.8 Calculation of indices**

369 The GDGT-0/crenarchaeol ratio was calculated to assess potential contributions to iGDGT
370 production from methanogens (although GDGT-0 is not exclusive to them) and ammonia-
371 oxidising archaea (Blaga et al., 2009). Values > 2 have been proposed to indicate a substantial
372 methanogenic input (Blaga et al., 2009; Schouten et al., 2013; Zell et al., 2014).

$$373 \text{GDGT-0/cren} = [\text{GDGT-0}] / [\text{crenarchaeol}]$$

374 The GDGT-2/crenarchaeol (GDGT-2/cren) index is used as an additional screening tool to
375 assess a potential AOM contribution (Weijers et al., 2011). An elevated GDGT-2/cren ratio
376 suggests increased synthesis of GDGT-2 within the SMI, likely from methanotrophic
377 Euryarchaeota (Pancost et al., 2001; Wakeham et al., 2003; Stadnitskaia et al., 2005).

378 $GDGT-2/cren = [GDGT-2] / [crenarchaeol]$

379 The Methane Index (MI) is based on GDGT-1 to GDGT-3 and crenarchaeol, and reflects the
380 balance between methanotrophic Euryarchaeota and Nitrososphaeria, whether planktonic or
381 benthic (Zhang et al., 2011). GDGTs associated with methanotrophs — mainly GDGT-1 to
382 GDGT-3 (Pancost et al., 2001; Zhang et al., 2011) — are primarily produced by ANME-1
383 (Rossel et al., 2008). The MI ranges from 0 to 1, with higher values (>0.3-0.5) indicating a
384 greater relative contribution of GDGT-1 to GDGT-3 than of crenarchaeol and cren', and are
385 linked to high methane fluxes (Kim and Zhang, 2023). The MI, as defined by Zhang et al.
386 (2011), was calculated as follows:

387 $MI = [GDGT-1 + GDGT-2 + GDGT-3] / [GDGT-1 + GDGT-2 + GDGT-3 + cren + cren']$

388 The Branched and Isoprenoid Tetraether index (BIT) estimates the relative contribution of
389 branched GDGTs to the combined pool of branched GDGTs and crenarchaeol, following
390 Hopmans et al. (2004), and serves as an indicator of terrestrial organic matter input into a marine
391 environment. However, brGDGTs may also be produced in situ in aquatic and sedimentary
392 environments (Peterse et al., 2009; Dearing Crampton-Flood et al., 2019 and references
393 therein). The BIT index ranges from 0 to 1, with higher values indicating a greater relative
394 contribution of brGDGTs compared with crenarchaeol:

395 $BIT = [brGDGT-Ia + II-a + IIIa] / [br-GDGT-Ia + IIa + IIIa + cren]$

396 The percentage of OH-GDGTs reflects the relative contribution of hydroxylated iGDGTs to the
397 total iGDGT pool and indicates an increased contribution from OH-GDGT-producing archaea
398 and/or adaptation to low temperature and salinity. The index was calculated following Huguet
399 et al. (2013):

400 $OH-GDGT\% = \frac{\Sigma[OH-GDGT-0 + OH-GDGT-1 + OH-GDGT-2]}{\{\Sigma[OH-GDGT-0 + OH-$
401 $GDGT-1 + OH-GDGT-2] + \Sigma[GDGT-0 + GDGT-1 + GDGT-2 + GDGT-3 + cren + cren']\}} \times$
402 100

403 The ring indices of hydroxylated tetraethers (RI-OH and RI-OH') quantify the degree of
404 cyclisation, that is, the number of cyclopentane rings in the molecules. This number increases
405 with temperature and decreases with salinity (Sinninghe Damsté et al., 2022). The RI-OH' is

406 more sensitive in cold regions (Varma et al., 2024). The indices were calculated following Lü
407 et al. (2015):

$$408 \text{ RI-OH} = \{[\text{OH-GDGT-1}] + 2 \times [\text{OH-GDGT-2}]\} / \{[\text{OH-GDGT-1}] + [\text{OH-GDGT-2}]\}$$

$$409 \text{ RI-OH}' = \{[\text{OH-GDGT-1}] + 2 \times [\text{OH-GDGT-2}]\} / \Sigma[\text{OH-GDGTs}]$$

410 **3 Results**

411 **3.1 Porewater profiles of SO_4^{2-} , CH_4 , and Cl^-**

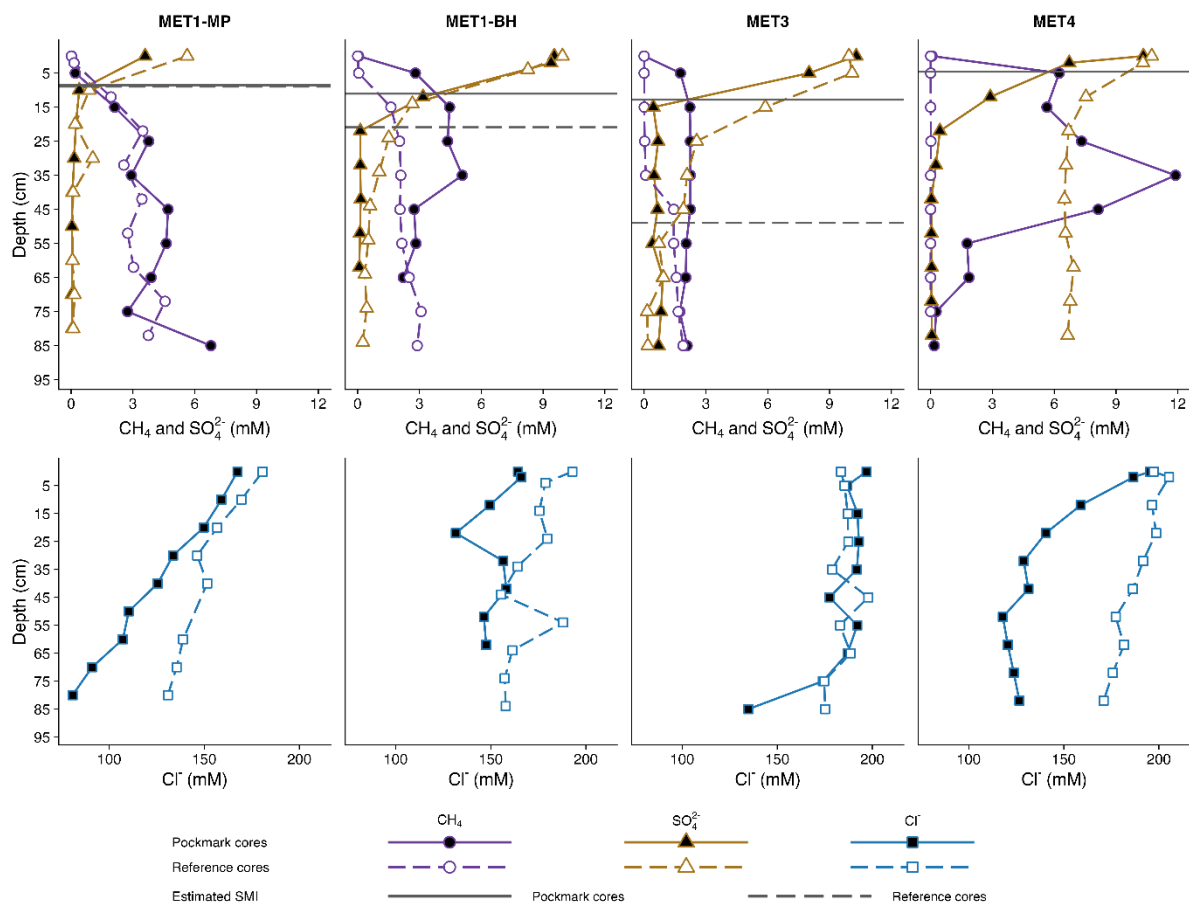
412

413 Pockmarks across all sites show greater sulphate depletion, with a mean SO_4^{2-} concentration
414 $1.5\times$ lower than in non-pockmarks (1.93 ± 3.33 SD mM vs 3.78 ± 3.72 SD mM, respectively,
415 Fig. 2). Although SO_4^{2-} concentrations span similar value ranges in pockmarks and non-
416 pockmarks ($0.03\text{--}10.33$ mM vs $0.07\text{--}10.73$ mM, respectively), their median values differ
417 substantially by a factor of ~ 5 (0.39 vs 1.99 mM, respectively). Pockmarks also show SO_4^{2-}
418 depletion occurring closer to the surface, meaning the depth at which SO_4^{2-} first drops below 1
419 mM (at 17.3 ± 5.9 cm in pockmark cores compared with 36.3 ± 23.5 cm in reference cores) and
420 0.5 mM (17.3 ± 5.9 cm in pockmark cores compared with 49.7 ± 27.8 cm in reference cores) is
421 2 and $3\times$ shallower, respectively. Pockmarks show mean CH_4 concentrations 2.3-fold higher
422 than at reference sites (3.1 ± 2.6 mM vs 1.3 ± 1.4 mM, mean \pm SD; Fig. 2). Median CH_4
423 concentrations were also higher in pockmark-cores (2.24 vs 1.44 mM; on average 3.11 ± 2.56
424 mM vs. 1.34 ± 1.38 mM), reflecting the influence of particularly high CH_4 concentrations in
425 selected pockmark horizons (ranging 0 – 11.89 mM) compared with non-pockmark ones (0 –
426 4.56 mM). MET4 exhibits the most extreme values across the examined sites and the greatest
427 differences between pockmark and reference cores; CH_4 reached the highest values in the
428 pockmark core, whereas the reference core remained close to CH_4 -free. By contrast, MET3
429 shows the least differentiation between pockmark and reference cores and has lower overall
430 methane concentrations.

431

432 Sulphate and CH_4 show clear, opposing depth trends across all four study locations, except at
433 non-pockmark S/MET4, where CH_4 is absent, and sulphate is high throughout the profile (Fig.
434 2). SO_4^{2-} is initially high in surface sediments and declines with depth, whereas CH_4 shows the
435 opposite pattern. For the purpose of this study, the SMI is defined as the layer within the
436 sediment at which the porewater concentrations of SO_4^{2-} and CH_4 are equal. At this interface,
437 AOM couples SO_4^{2-} reduction to CH_4 oxidation, consuming most of the CH_4 and SO_4^{2-} and

438 producing low concentrations of both. The depth of SMI, as well as the differences between
 439 pockmark and reference sites, vary by location, with SMI in pockmarks located closer to the
 440 sediment surface (Fig. 2). In pockmark sediments, the SMI was located 5–15 cm below the
 441 seafloor, whereas in non-pockmark sediments it was 10–50 cm below the seafloor. At MET1-
 442 BH and MET3, the SMI in the pockmarks was shallower than at the reference stations; at
 443 MET1-MP, the SMI in the pockmark was similarly shallow to that at the reference site; at
 444 MET4, no SMI was detected within the sampled interval at the non-pockmark site, while the
 445 pockmark exhibited a shallow SMI.



446
 447 Fig. 2. Profiles of SO₄²⁻ and CH₄ differ in absolute concentrations across sites, with greater SO₄²⁻
 448 depletion occurring closer to the surface in pockmarks than in reference sites. Methane concentrations
 449 are, on average, approximately 2.3 times higher in pockmark cores than in reference cores, with the
 450 highest values at P/MET4. Dashed (reference cores) and solid (pockmark cores) horizontal lines indicate
 451 the SMI estimated at the point where porewater concentrations of SO₄²⁻ and CH₄ are equal. Depth
 452 profiles of porewater Cl⁻ at MET1-MP, MET1-BH, MET3, and MET4, ranging from 2863 to 7279 mg
 453 dm⁻³. The profiles consistently show higher Cl⁻ concentrations in reference sediments than in those in
 454 pockmark sediments. The extent and shape of these profiles vary across sites. The most distinct

455 separation between pockmark and reference profiles occurs at MET4 and MET1-MP, whereas MET3
456 shows substantial overlap. Depth is given in cm below the sea floor (bsf).

457

458 Chloride porewater profiles differed among the investigated sites, with generally lower
459 concentrations in pockmark cores (151.39 ± 31.13 mM) than in reference cores (174.84 ± 18.43
460 mM) (Fig. 2).

461

462 The strongest contrast between the pockmark and reference cores is evident at MET4 (Fig. 2).
463 This contrast reflects a pronounced downcore Cl^- depletion in the P/MET4 pockmark core (from
464 195.40 mM at the surface to 117.97–126.66 mM below 50 cm depth), compared with the
465 reference core, which shows consistently higher and steady Cl^- concentrations (170.94–205.33
466 mM). This pattern indicates freshwater enrichment within the P/MET4 pockmark core relative
467 to the adjacent reference core. However, the lowest concentrations occur in the MET1-MP
468 pockmark core, where Cl^- decreases steadily with depth (from 167.50 mM at the surface to
469 80.76 mM at the bottom). Whereas Cl^- concentrations also decrease with depth in the reference
470 core of MET1-MP (ranging 130.86–180.71 mM), they remain higher than in the MET1-MP
471 pockmark core (Fig. 2). In the MET1-BH pockmark core, Cl^- concentrations are lower than in
472 the reference core throughout the sediment profile, but the pattern is irregular (a dip to 131.65
473 mM at 20 cm and a recovery to ~147–158 mM below). In the MET1-BH reference core, Cl^-
474 concentrations are higher and more variable (155.49–192.89 mM). At MET3, the pockmark
475 and reference cores are largely similar across the depth profile and remain among the highest
476 Cl^- levels in the dataset (134.87–196.98 mM, median 189.44 ± 18.24 vs 174.67 – 197.88 mM,
477 median 184.44 ± 6.9 , respectively). The main difference appears in the deepest P/MET3
478 pockmark sample, where the Cl^- concentration drops (134.87 mM at 85 cm), whereas the
479 reference core remains constant (Fig. 2).

480

481 **3.2 LOI**

482

483 LOI-derived estimates of organic matter are sensitive to ignition conditions and sediment
484 composition. Because mass loss at 550 °C may include contributions from sediment
485 mineralogy, including inorganic carbon-bearing minerals, LOI-based values provide a
486 screening-level estimate of TOC rather than an exact measurement of organic matter content.
487 To assess whether LOI captured the main downcore stratigraphic trends in organic carbon, LOI

488 profiles were compared with directly measured TOC in two representative cores: the MET1-
489 MP pockmark core and the MET3 reference core (Supplementary material Fig. S2).

490

491 Consistent with the regional relationship between TOC and LOI reported in the Gdańsk Basin
492 by Łukawska-Matuszewska et al. (2014) across all paired measurements, TOC and LOI in the
493 pockmark core P/MET1-MP and the reference core S/MET3 are significantly correlated ($r =$
494 0.65 , $p < 0.005$), and linear regression explains 43% of the variability in TOC ($R^2 = 0.43$; TOC
495 $= 0.612 + 0.282 \text{ LOI}$). The positive correlation between LOI and TOC supports using LOI as a
496 proxy for organic matter variability. In both cores, intervals of increased LOI predominantly
497 coincide with higher measured TOC, demonstrating that LOI reliably reflects variations in
498 organic matter content, despite differences (Supplementary material Fig. S2).

499

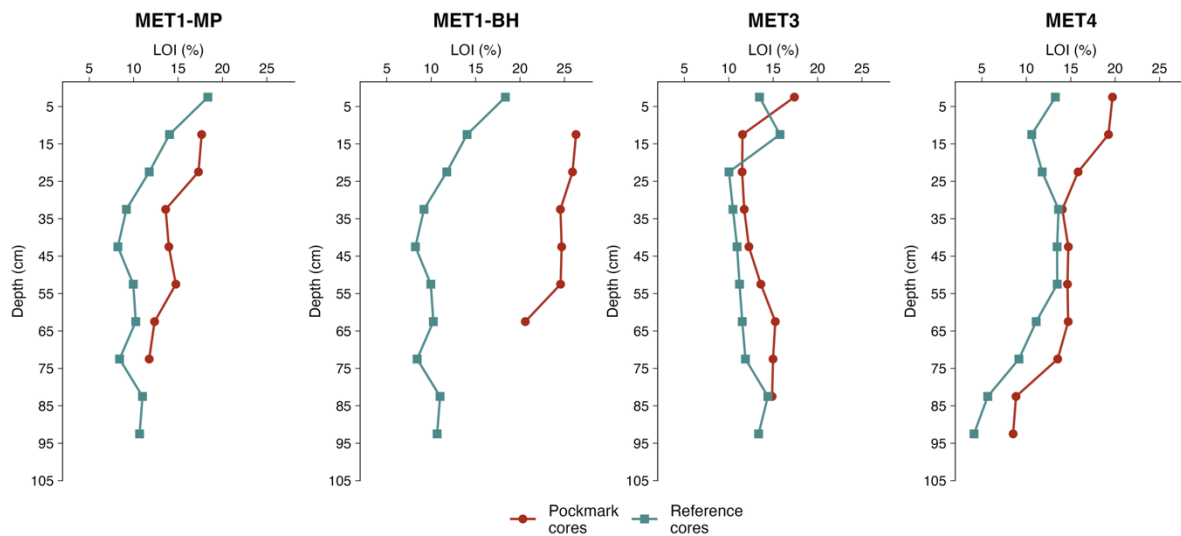
500 In the MET1-MP pockmark core, both LOI and measured TOC are relatively elevated in the
501 upper to middle part of the core and generally decrease below ~45-55 cm depth (Supplementary
502 material Fig. S2). This indicates a downcore decline in bulk organic matter content below the
503 mid-core interval. In the S/MET3 reference core, measured TOC is highest in the shallowest
504 interval, decreases through the upper-middle section of the core, and subsequently increases in
505 deeper intervals, while LOI follows a comparable vertical pattern (Supplementary material Fig.
506 S2). Therefore, LOI is used below as a qualitative, high-resolution proxy for bulk organic matter
507 trends in the studied cores, providing a sedimentary and geochemical context for the GDGT
508 and microbial distributions.

509

510 LOI values show site-specific and downcore variability, with varying degrees of contrast
511 between pockmark and reference cores, indicating differences in bulk organic matter content
512 and relative enrichment in pockmark cores, especially pronounced in MET1-BH (Fig. 3). In the
513 MET1 area, the same reference core was used for comparison with the MET1-MP and MET1-
514 BH pockmarks. LOI values were elevated in pockmark cores compared with reference cores,
515 particularly in MET1-BH and MET1-MP, with LOI values on average approximately 2.2-fold
516 higher in the MET1-BH pockmark core and 1.3-fold higher in the MET1-MP pockmark core
517 relative to the shared MET1 reference core. The strongest enrichment occurs at MET1-BH,
518 where pockmark LOI values are about 1.9-3.0 times higher than the corresponding reference
519 values. In contrast, pockmark P/MET3 shows only a weak average difference of ~1.1-fold, with
520 depth-wise ratios ranging from 0.7 to 1.3, indicating that LOI values at MET3 are broadly
521 overlapping between pockmark and reference cores.

522
523
524
525
526
527
528
529
530

At MET4, pockmark LOI values were on average ca. 1.4-fold higher than in the reference core, with the relative difference elevated in the uppermost part of the profile (10-15 cm), decreasing below that section, and increasing again in the middle part of the profile, reaching approximately 2.1-fold in the deepest interval of the profile, where the reference core shows low LOI values of ~4% (Fig. 3). The LOI results, used as a proxy for organic matter content, indicate that organic matter accumulation is site-specific and should not be generalised across all pockmarks.



531
532
533
534
535
536
537
538
539
540
541
542
543

Fig. 3. Downcore variation of loss-on-ignition (LOI%) in sediment cores collected from the Gulf of Gdańsk (MET1-MP, MET1-BH) and the Gdańsk Deep (MET3, MET4), south-eastern Baltic Sea. LOI values are plotted against depth bsf and serve as a qualitative, screening-level proxy for variability in bulk organic matter. Pockmark sediments are compared with adjacent reference (non-pockmark) sediment cores at each site; for the MET1-MP and MET1-BH pockmarks, the same reference core is used. LOI values are elevated in the pockmark cores at MET1-MP, MET1-BH, and MET4, with the strongest enrichment observed at MET1-BH. By contrast, MET3 shows values that are approximately overlapping between the pockmark and reference sediment cores. At MET4, both cores show a pronounced downcore decrease in LOI, particularly in the reference core, where values decline to ca. 4% in the deepest part of the profile.

3.3 iGDGTs in pockmark and non-pockmark marine surface sediments

544 The abundance and distribution of iGDGTs (GDGT-0 to GDGT-3, crenarchaeol, and its isomer)
545 were analysed in pockmark core sediments and in surrounding non-pockmark reference core
546 sediments (Fig. 4). All targeted iGDGTs were detected in both settings.

547 Unless stated otherwise, concentration values are reported as ranges, followed by the median
548 and the mean \pm standard deviation (SD). Summed iGDGT concentrations (Σ iGDGTs) span
549 0.02–58.85 $\mu\text{g g}^{-1}$ sediment across all samples, with values generally higher and more variable
550 in pockmark sediment cores (0.92–58.85 $\mu\text{g g}^{-1}$ sediment; 5.10 $\mu\text{g g}^{-1}$; 10.58 \pm 13.08 $\mu\text{g g}^{-1}$)
551 than in reference sediment cores (0.02–16.81 $\mu\text{g g}^{-1}$ sediment; 2.59 $\mu\text{g g}^{-1}$; 3.73 \pm 3.41 $\mu\text{g g}^{-1}$),
552 that is, approximately twice the median and three times the mean. Spatially, the highest
553 Σ iGDGT concentrations occur at sites in the Gdańsk Deep (MET3, MET4), whereas lower
554 concentrations are generally observed in the MET1 area (Fig. 4). With depth, Σ iGDGTs
555 commonly show shallow to mid-depth maxima, particularly between approximately 15 and 45
556 cm bsf, followed by downcore depletion. Excluding the anomalously low values in the S/MET4
557 reference core, Σ iGDGTs concentrations typically decline by a factor of \sim 2.6 to \sim 64, although
558 the fold decrease is much larger where the deepest reference intervals approach near-zero values
559 in S/MET4.

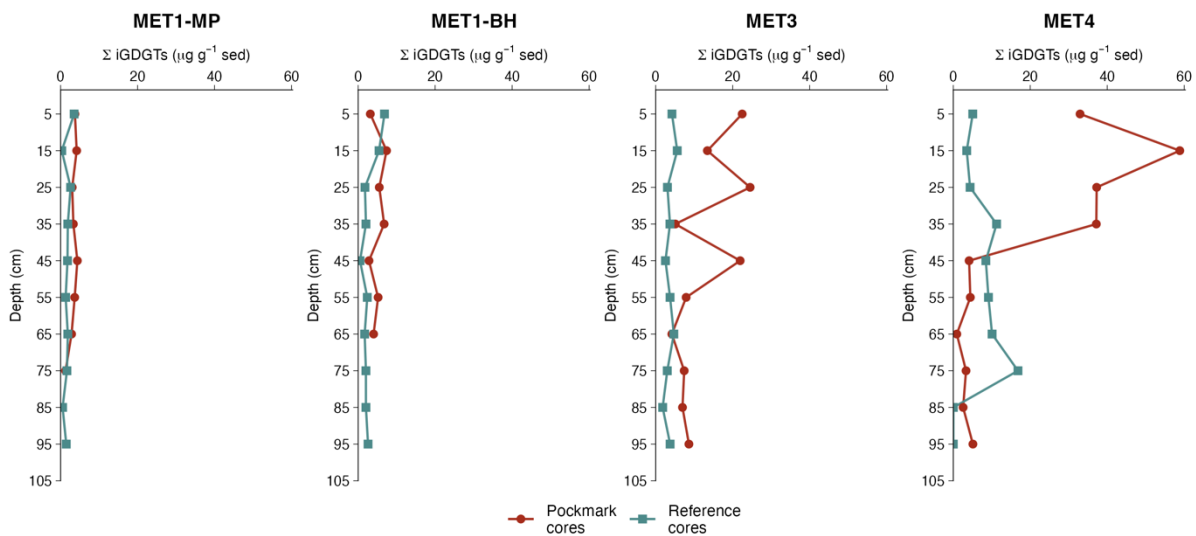
560 Crenarchaeol (cren) is the dominant iGDGT in both pockmark cores (mean fractional
561 abundance of 0.53 \pm 0.03 SD) and reference cores (0.55 \pm 0.02 SD) (Fig. 5). GDGT-0 is the
562 second most abundant in pockmark and reference cores (0.43 \pm 0.03 SD; 0.41 \pm 0.02 SD,
563 respectively) (Fig. 5). Together, crenarchaeol and GDGT-0 account for \sim 96 % of the total
564 iGDGT pool in both pockmark and reference cores, indicating broadly similar iGDGT
565 distributions between pockmarks and references. Consistently, GDGT-0 covaries very strongly
566 with crenarchaeol ($r = 0.996$, $p < 0.001$).

567 The remaining iGDGTs, GDGT-1 to GDGT-3, occur only in minor proportions and at much
568 lower concentrations (Fig. 5). Across the analysed depth intervals from 0-5 to 90-95 cm bsf,
569 GDGT-1, GDGT-2, and GDGT-3 show a highly consistent pattern of relative abundance. In 74
570 of 75 samples, the order is GDGT-1 > GDGT-2 > GDGT-3, and GDGT-2 is not the dominant
571 compound in any sample. The only exception is sample P/MET4/3, where the order is GDGT-
572 1 > GDGT-3 > GDGT-2.

573 Concentration profiles of the individual iGDGTs (Supplementary material Fig. S4) generally
574 follow similar downcore patterns, except for isolated concentration maxima of GDGT-1 in

575 P/MET1-BH/6 and GDGT-3 in P/MET4/3, minor changes in the crenarchaeol isomer (cren') at
 576 MET1-MP and MET1-BH, and even smaller differences at MET3 and MET4. GDGT-1,
 577 GDGT-2, and GDGT-3 also show strong covariation with crenarchaeol ($r = 0.988, 0.954, 0.951,$
 578 $p < 0.001$). Across all iGDGT pairs, correlations are consistently strong ($r = 0.847\text{--}0.996, p <$
 579 0.001), indicating that the individual iGDGTs vary largely in concert rather than exhibiting
 580 compound-specific enrichments.

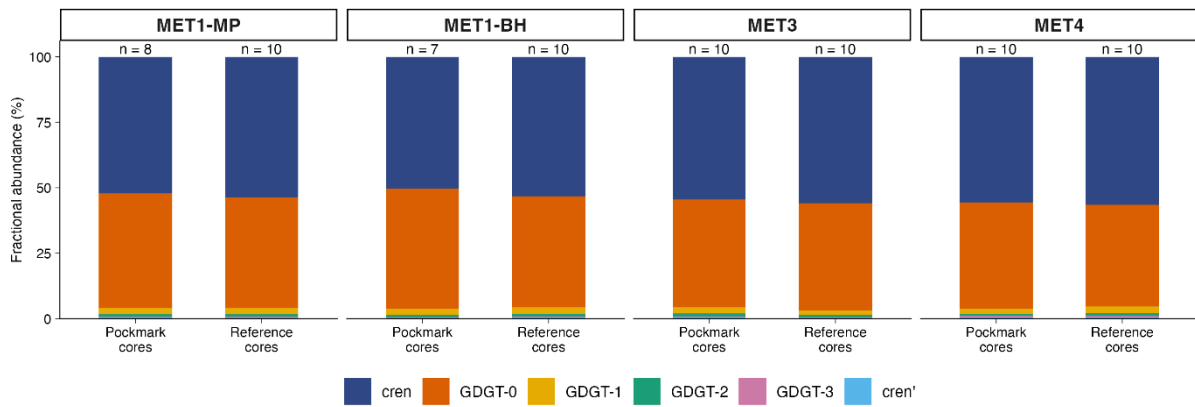
581 The mean \pm SD values for the indices are reported in Table 1. The GDGT-0/cren ratio is
 582 moderate and broadly comparable between pockmark and reference cores, ranging from 0.65
 583 to 0.99 in pockmark cores and from 0.63 to 0.91 in reference cores (downcore variability shown
 584 in supplementary material, Fig. S3). No consistent downcore trend is observed across all cores;
 585 where changes occur, they are site-specific and modest relative to the overlap between
 586 pockmark and reference cores. The GDGT-2/cren ratio is consistently low (0.01–0.04), and MI
 587 values remain low, ranging from 0.04 to 0.09 in pockmarks and from 0.03 to 0.07 in references.
 588 The BIT index values are generally low, ranging from 0.008 to 0.14 in pockmarks and from
 589 0.034 to 0.47 (to 0.17 without two S/MET4/9-10 outliers) in references, with the slightly higher
 590 values in reference cores.



591
 592 Fig. 4. Downcore profiles of summed isoprenoidal glycerol dialkyl glycerol tetraethers (Σ iGDGTs; μg
 593 g^{-1} dry sediment) for sediment cores from four sites in the south-eastern Baltic Sea: MET1-MP and
 594 MET1-BH (Gulf of Gdańsk), and MET3 and MET4 (Gdańsk Deep). Concentrations are plotted as a
 595 function of depth bsf, showing a general downcore decrease. Σ iGDGTs exhibit elevated concentrations
 596 in pockmark sediment cores relative to adjacent reference sediment cores, with the most pronounced
 597 enrichment observed at the Gdańsk Deep sites (MET3, MET4), where elevated near-surface values are

598 followed by a downcore decrease. Error bars are not shown because each point represents a single
 599 sediment horizon analysed once (see Section 2.5).

600



601
 602 Fig. 5. Mean fractional abundances of iGDGTs in pockmark and reference cores at sites MET1-MP,
 603 MET1-BH, MET3, and MET4 in the south-eastern Baltic Sea. Stacked bars show mean fractional
 604 abundances of iGDGTs (GDGT-0–3, crenarchaeol, and cren'), averaged by site and core type; n
 605 indicates the number of horizons (samples). The upper panel shows the full scale (0–100%).
 606 Crenarchaeol and GDGT-0 dominate across all sites, whereas GDGT-1–3 and cren' constitute minor
 607 fractions.

608
 609 Table 1. Mean GDGT-based indices for pockmark (P) and reference (S) sediment cores at MET1 (MP,
 610 BH), MET3, and MET4. Values are reported as mean \pm sample standard deviation, rounded to a
 611 maximum of two significant figures. Metrics include OH-GDGT%, hydroxylated GDGT ring indices
 612 (RI-OH, RI-OH'), the Branched and Isoprenoid tetraether index (BIT), the Methane Index (MI), and
 613 diagnostic ratios (GDGT-0/cren, GDGT-2/cren). RI-OH shows minimal variation across sites and
 614 between pockmark and reference cores (\sim 1.1–1.2), indicating comparable OH-GDGT cyclisation
 615 patterns. OH-GDGT% is moderately elevated at MET1 relative to MET3–MET4, with minimal within-
 616 site variation. MI values remain consistently low (0.05–0.07). GDGT-0/cren ratios are consistently
 617 slightly elevated in pockmark cores relative to paired references, whereas GDGT-2/cren remains
 618 uniformly low (0.01–0.02), indicating that pockmark influence primarily affects GDGT-0 abundance
 619 rather than higher-cyclised GDGTs. Downcore variability of MI, BIT, RI-OH, RI-OH', and GDGT-
 620 0/cren is shown in the supplementary material (Fig. S3).

621

Sediment core	OH-GDGT%	RI-OH	RI-OH'	BIT	MI	GDGT-0/cren	GDGT-2/cren
P/MET1-MP	9.0 \pm 0.4	1.2 \pm 0.03	0.19 \pm 0.02	0.12 \pm 0.01	0.065 \pm 0.003	0.84 \pm 0.02	0.019 \pm 0.001
P/MET1-BH	9.3 \pm 0.4	1.2 \pm 0.04	0.19 \pm 0.02	0.09 \pm 0.01	0.066 \pm 0.003	0.92 \pm 0.04	0.019 \pm 0.002

P/MET3	7.9±0.9	1.2±0.02	0.21±0.03	0.05±0.02	0.064±0.008	0.76±0.11	0.021±0.004
P/MET4	7.8±1.3	1.1±0.02	0.19±0.02	0.03±0.02	0.054±0.016	0.74±0.08	0.014±0.003
S/MET1-MP	8.1±0.8	1.2±0.04	0.25±0.04	0.14±0.03	0.066±0.002	0.79±0.05	0.019±0.001
S/MET1-BH	8.1±0.9	1.2±0.02	0.23±0.03	0.12±0.02	0.066±0.003	0.80±0.06	0.019±0.001
S/MET3	7.0±0.6	1.2±0.03	0.19±0.02	0.07±0.01	0.047±0.003	0.73±0.07	0.013±0.001
S/MET4	7.2±0.9	1.2±0.06	0.21±0.07	0.13±0.16	0.065±0.036	0.69±0.03	0.019±0.013

622

623 **3.4 OH-GDGTs in pockmark and non-pockmark sediments**

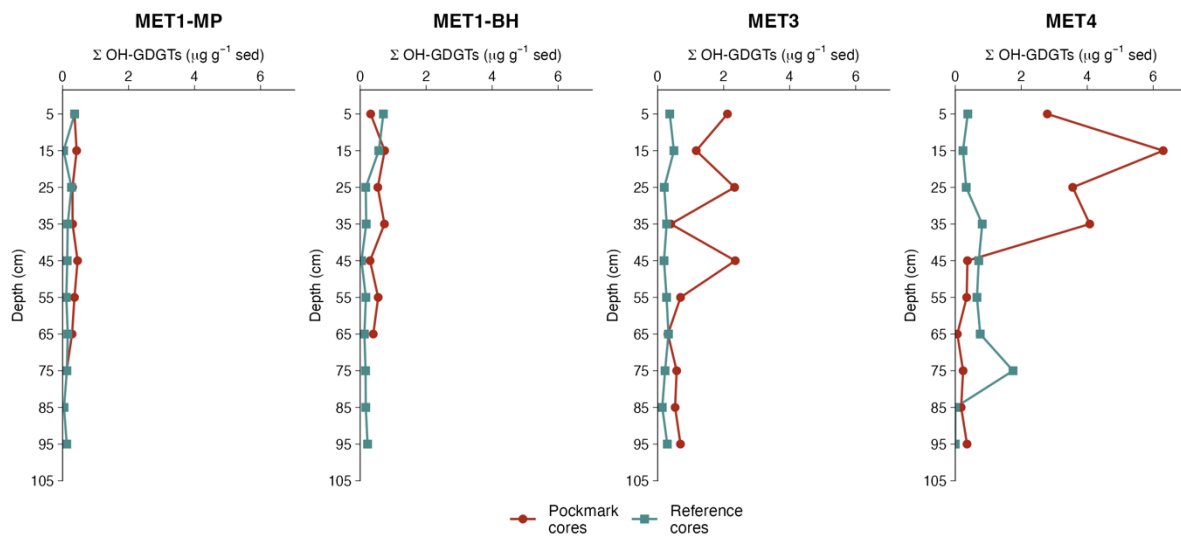
624 The abundance and distribution of hydroxylated GDGTs (OH-GDGT-0 to -2) in pockmark and
625 reference cores broadly mirror those of iGDGTs, with strong positive cross-correlations ($r =$
626 $0.840\text{--}0.992$, $p < 0.001$) and the tightest coupling with GDGT-0 ($\Sigma\text{OH-GDGTs}$: $r = 0.992$, $p <$
627 0.001) and crenarchaeol ($r = 0.983$, $p < 0.01$). All targeted OH-GDGTs (OH-GDGT-0 to -2)
628 were detected in both settings.

629 Summed OH-GDGT concentrations ($\Sigma\text{OH-GDGTs}$) ranged from 0.00 to 6.30 $\mu\text{g g}^{-1}$ sediment
630 across all samples, with values generally higher in pockmark sediment cores (0.06–6.30 $\mu\text{g g}^{-1}$
631 sediment; $0.43 \mu\text{g g}^{-1}$ sediment; $1.02 \pm 1.36 \mu\text{g g}^{-1}$ sediment) than in reference sediment cores
632 (0.00–1.75 $\mu\text{g g}^{-1}$ sediment; $0.21 \mu\text{g g}^{-1}$ sediment; $0.31 \pm 0.32 \mu\text{g g}^{-1}$ sediment) (Fig. 6). $\Sigma\text{OH-}$
633 GDGTs are therefore, on average, approximately three times higher and, at the median, about
634 twice as high in pockmarks as in references. Spatially, the highest $\Sigma\text{OH-GDGTs}$ concentrations
635 occur at MET4, intermediate values at MET3, and lower values in the MET1 area, broadly
636 mirroring the spatial pattern observed for ΣiGDGTs . With depth, $\Sigma\text{OH-GDGTs}$ commonly
637 show shallow to mid-depth maxima, typically between 15 and 45 cm bsf, followed by downcore
638 depletion (Fig. 6). This decrease is particularly pronounced at MET4, especially in P/MET4,
639 where ΣiGDGTs declined from 6.30 to 0.06 $\mu\text{g g}^{-1}$ sediment.

640 Across all cores, OH-GDGTs are dominated by OH-GDGT-0 in both pockmark and reference
641 cores (Fig. 7, average fractional abundances of 0.83 ± 0.02 SD and 0.82 ± 0.03 SD, respectively).
642 OH-GDGT-1 and OH-GDGT-2 are consistently minor components (Fig. 7). Overall, OH-
643 GDGT distributions are broadly similar between pockmark and reference cores (Supplementary
644 material Fig. S5), and most variability is evident in downcore concentration profiles, which
645 typically decline by a factor of ~ 1.2 to ~ 7.8 , with most cores showing an average decrease by a
646 factor of ~ 3 (except for S/MET4, which declines to zero at the base). Across all OH-GDGT
647 pairs (OH-0, OH-1, OH-2), correlations are consistently very strong ($r = 0.975\text{--}0.992$, $p < 0.01$).

648 OH-GDGT% and RI-OH show only minor differences between pockmark and reference cores
 649 (Table 1). OH-GDGT% values are slightly higher in pockmarks (6.4–9.9) than in references
 650 (6.2–9.4). RI-OH is identical between settings (1.1–1.3 in pockmarks; 1.1–1.3 in references),
 651 whereas RI-OH' is modestly higher in references (0.16–0.36) than in pockmarks (0.16–0.25).
 652 Overall, variability in OH-GDGTs is mainly reflected in absolute abundances, while OH-
 653 GDGT distribution and indices are broadly comparable between pockmark and reference cores.

654

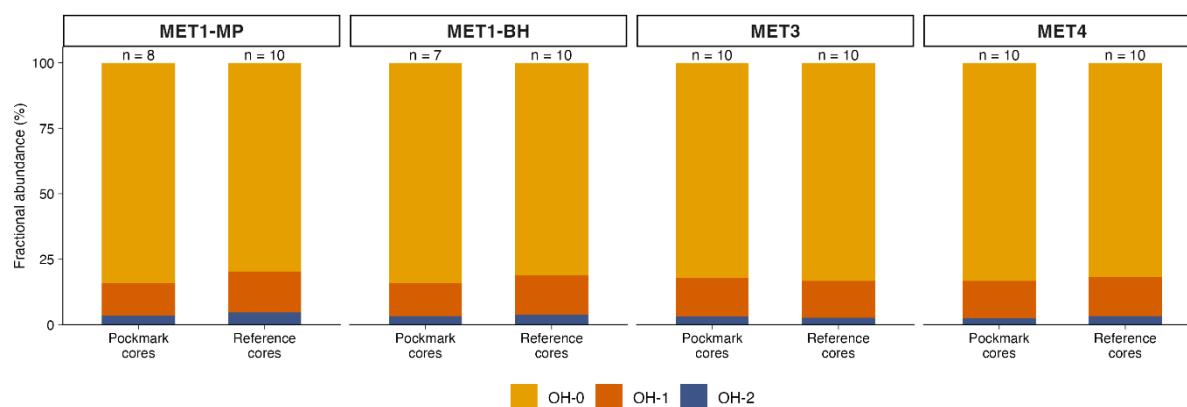


655

656 Fig. 6. Downcore profiles of summed hydroxylated glycerol dialkyl glycerol tetraethers (Σ OH-GDGTs;
 657 $\mu\text{g g}^{-1}$ dry sediment) for sediment cores from four sites in the south-eastern Baltic Sea: MET1-MP and
 658 MET1-BH (Gulf of Gdańsk) and MET3 and MET4 (Gdańsk Deep). Concentrations are plotted against
 659 depth (downcore increase; cm). Σ OH-GDGT concentrations follow the pattern of iGDGTs, showing
 660 strong positive cross-correlations and the highest coupling with GDGT-0 and crenarchaeol (see Section
 661 3.2). In the Gulf of Gdańsk (MET1-MP, MET1-BH), Σ OH-GDGTs show lower overall abundances than
 662 iGDGTs but remain elevated in pockmark intervals relative to reference sediments.

663

664



665
 666 Fig. 7. Mean OH-GDGT fractional abundances in pockmark versus reference cores at sites MET1-MP,
 667 MET1-BH, MET3, and MET4 in the south-eastern Baltic Sea. Stacked bars show mean fractional
 668 abundances of OH-0, OH-1 and OH-2, averaged by site and core type (pockmarks and references); n
 669 denotes the number of horizons (samples). OH-0 dominates across all sites, with OH-1 contributing a
 670 smaller yet consistent fraction and OH-2 occurring at low abundance.

671
 672 **3.5 Abundance and composition of archaea**

673
 674 Archaeal community composition differs between pockmark and reference sediments (Fig. 8).
 675 However, at the class level, most samples are dominated by Nanoarchaeia (Fig. 8a). Additional
 676 major contributions, at varying proportions, include Thermoplasmata, Methanosarcinia,
 677 Thermococci, Bathyarchaeia, Lokiarchaeia, and Methanomicrobia (Fig. 8a). Pockmark samples
 678 generally contain higher proportions of methane-cycling archaeal groups, particularly
 679 Methanosarcinia and Methanomicrobia, whereas reference cores more commonly show
 680 elevated contributions of Thermoplasmata, Bathyarchaeia, and Lokiarchaeia (Fig. 8a). The
 681 general depth trend shows Nanoarchaeia dominating shallower horizons, uniformly across
 682 reference and pockmark cores. Nanoarchaeia dominate the archaeal community in pockmarks,
 683 even in deeper sediment horizons, particularly at P/MET1-BH and P/MET1-MP. Vertical
 684 stratification is less consistent and more site-specific in pockmark cores than in reference cores,
 685 but the relative abundance of Methanosarcinia, Thermococci, and Bathyarchaeia increases
 686 downcore. Methanomicrobia also show a pockmark-associated pattern, with higher mean
 687 relative abundance in pockmarks than in references ($2.6 \pm 1.8\%$ vs. $0.6 \pm 1.0\%$, respectively),
 688 indicating additional methanogen-affiliated archaeal populations beyond Methanosarcinia (Fig.
 689 8a). In reference cores, in deeper horizons, the community composition shifts towards a higher
 690 relative abundance of Thermoplasmata, Bathyarchaeia, Lokiarchaeia, and Deep Sea
 691 Euryarchaeotic Group (DSEG, currently within Thermoplasmata; Rinke et al., 2021),

692 suggesting a greater contribution from uncultivated anaerobic sedimentary archaeal lineages
693 with depth. Across all samples, these classes were more abundant in reference than in pockmark
694 cores, with mean relative abundances of $20.5 \pm 13.6\%$ vs $9.4 \pm 5.2\%$ for Thermoplasmata, 14.8
695 $\pm 19.5\%$ vs $5.2 \pm 5.9\%$ for Bathyarchaeia, $5.6 \pm 2.4\%$ vs $3.5 \pm 2.6\%$ for Lokiarchaeia, and 3.0
696 $\pm 1.7\%$ vs $2.0 \pm 1.8\%$ for DSEG.

697

698 Archaeoglobi were more abundant in reference sediments, averaging $1.7 \pm 1.9\%$ and $0.4 \pm$
699 0.6% , respectively, particularly in mid-depth horizons, where they may indicate a sulphur-
700 cycling anaerobic archaeal community (Fig. 8a). Other low-abundance classes, including
701 Micrarchaeia, Iainarchaeia, Altiarchaeia and Heimdallarchaeia, formed part of the archaeal rare
702 biosphere and exhibited localised enrichment in selected horizons. ANME-1 was detected only
703 at trace relative abundance.

704

705 Nitrososphaeria were detected in both pockmark and reference cores, with taxonomic profiling
706 revealing that this class is dominated almost exclusively by Nitrosopumilaceae (Fig. 8e,
707 supplementary material Fig. S6) and, at the genus level, primarily by *Candidatus*
708 *Nitrosopumilus* (Supplementary material Fig. S7a, b). Nitrosopumilaceae showed higher
709 relative abundance in reference cores ($14.0 \pm 8.8\%$) than in pockmark cores ($8.8 \pm 3.7\%$), with
710 maxima in deeper reference sediment strata. *Ca.* *Nitrosopumilus* was more abundant in
711 reference cores, particularly in S/MET3/10, S/MET1-MP/10, and S/MET1-BH/10
712 (Supplementary material Fig. S7a, b). These distributional trends indicate that
713 Nitrosopumilaceae-affiliated AOA are a more significant component of the biogeochemical
714 nitrogen-cycling community in non-pockmark and deeper sediment horizons, whereas selected
715 pockmark layers are comparatively enriched in archaeal taxa implicated in CH₄ cycling. This
716 indicates that the distinction between pockmark and reference sediments is largely reflected in
717 shifts in the relative abundance of CH₄-cycling, heterotrophic/fermentative, and ammonia-
718 oxidising archaeal groups.

719

720 Hierarchical analysis at the class level showed four distinct clusters (Fig. 8b), with partial
721 clustering of pockmark and reference samples and overlap between the pockmark and reference
722 cores. Cluster 1 comprises the pockmark samples; Cluster 2 combines reference and pockmark
723 samples; Cluster 3 groups mainly reference samples; and Cluster 4 comprises two S/MET1-BH
724 reference samples and the P/MET4/10 sample (outliers). This pattern is consistent with the
725 MDS ordination. The PERMANOVA test (Fig. 8c) indicates that the difference between

726 pockmark and reference archaeal communities is statistically significant ($p = 0.003$).
727 Multivariate analysis using MDS clearly shows clustering of samples into two categories –
728 pockmarks vs references (Fig. 8c). However, some differences are noticeable: pockmark
729 samples are more tightly clustered, whereas reference samples are slightly more dispersed.
730 Based on the above analyses, it can be assumed that the pockmark cores differ significantly in
731 their archaeal composition from the adjacent reference cores. Additionally, PCA analysis
732 indicates the groups that may have the greatest impact on sample differentiation (Fig. 8d). For
733 pockmarks, the greatest impact on sample variability is as follows: Hadarchaeia >
734 Methanobacteria > Methanocellia > Halobacteria. In the reference samples, the order is
735 Methanocellia > ANME-1 > Methanobacteria > Hadarchaeia. In both pockmark and reference
736 cores, the same groups contribute most to sample variability, although the proportions of these
737 contributions differ; therefore, the compositions must differ.

738

739 Because several archaeal groups discussed in relation to methane cycling and ammonia
740 oxidation are not resolved at the class level, the family-level heatmap is presented to clarify the
741 distribution of key taxa (Fig. 8e). Additional figures in the supplementary material show
742 extended family-level relative abundance profiles (Supplementary material Fig. S6), the genus-
743 level heatmap with extended genus-level relative abundance profiles (Supplementary material
744 Fig. S7a, b), and profiles revealing the relative abundances of methanogenic (Supplementary
745 material Fig. S8) and methanotrophic (Supplementary material Fig. S9) archaeal groups.

746

747 At the family level, a few groups dominate both pockmark and reference cores, albeit in
748 different proportions: SCGC_AAA011-D5, uncultured lineages, GW2011, and
749 Nitrosopumilaceae (Fig. 8e). However, there are some site- and horizon-specific distinctions.
750 Pockmark cores are characterised by a strong, localised enrichment of methane-cycling archaea,
751 particularly ANME-2a-2b group (mean relative abundance of $5.5 \pm 9.3\%$ vs $1.8 \pm 3.1\%$),
752 Methanosarcinaceae ($5.0 \pm 6.0\%$ vs $3.4 \pm 1.9\%$), Methanomicrobiaceae ($2.2 \pm 1.8\%$ vs $0.3 \pm$
753 0.4%), and Methanosaetaceae ($1.8 \pm 1.5\%$ vs $0.8 \pm 1.6\%$). These taxa show vertical
754 heterogeneity, with relative abundances peaking at the middle and bottom of the profiles, i.e.,
755 ANME-2a-2b group in the deeper parts of the pockmark cores (P/MET1-MP/7, P/MET4/10;
756 Fig. 8e; Supplementary material Fig. S6), as well as Methanosarcinaceae (P/MET4/5; Fig. 8e;
757 Supplementary material Fig. S6) and Methanomicrobiaceae (P/MET4/5; Fig. 8e;
758 Supplementary material Fig. S6). Reference cores, by contrast, show a stronger contribution
759 from Nitrosopumilaceae ($14.0 \pm 8.8\%$ vs $8.8 \pm 3.7\%$), Archaeoglobaceae ($2.0 \pm 2.3\%$ vs $0.5 \pm$

760 0.7%), Hadarchaeales ($1.3 \pm 2.0\%$ vs $0.5 \pm 0.7\%$), and uncultured lineages ($25.3 \pm 21.1\%$ vs.
761 $10.1 \pm 7.4\%$) (Fig. 8e; supplementary material Fig. S6), which are characterised by variable
762 depth-related trends.

763

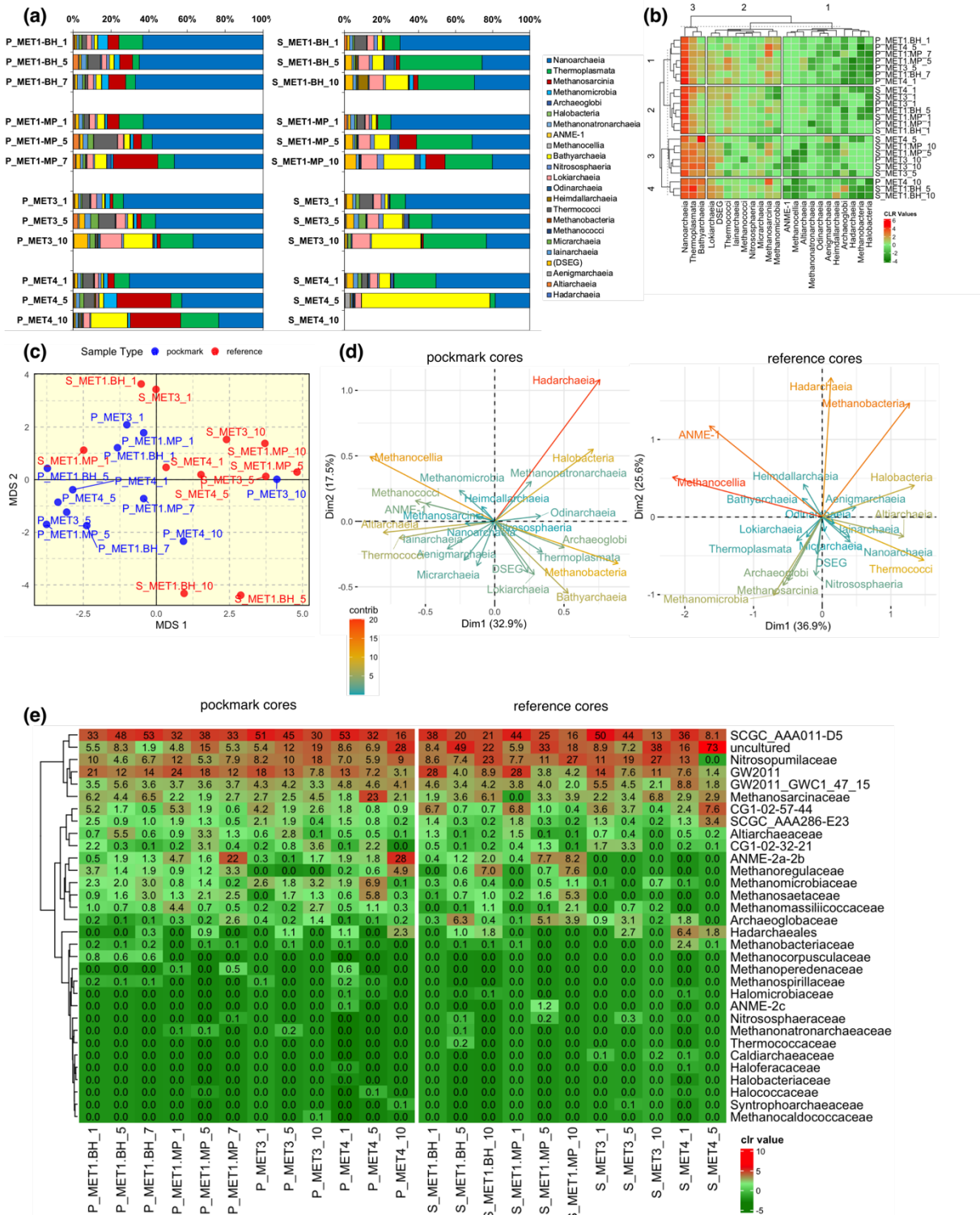
764 At the genus level, both pockmark and reference cores are dominated by AR15, *Ca.*
765 *Nitrosopumilus*, *Methanosarcina*, and AR20 (Supplementary material Fig. S7). However, the
766 archaeal community in pockmark cores shows a higher relative contribution of methanotrophic
767 taxa than in reference cores, i.e., ANME-3 (minor component; $0.7 \pm 1.0\%$ vs $0.1 \pm 0.4\%$),
768 particularly in cores P/MET1-BH and P/MET4, and ANME-2b ($7.5 \pm 12.3\%$ vs $1.9 \pm 4.1\%$),
769 particularly in the upper and lower parts of the profiles P/MET1-MP and P/MET4; as well as
770 enrichment of methanogens, particularly at mid-depth in P/MET4: *Methanosarcina* (29.3%),
771 *Methanosaeta* (8.2%), and *Methanogenium* (5.9%). In contrast, reference cores show a stronger
772 representation of *Ca. Nitrosopumilus* ($34.1 \pm 17.7\%$ vs $22.3 \pm 7.4\%$), particularly at mid-depth
773 in S/MET3, as well as AR20 ($7.5 \pm 6.1\%$ vs $2.4 \pm 1.8\%$) and *Methanoregula* ($3.3 \pm 6.1\%$ vs.
774 $2.8 \pm 3.5\%$), particularly at the bottom of the S/MET1-BH profile.

775

776 The methanogenic and methanotrophic groups are not restricted to pockmarks; in the reference
777 cores, their relative abundances are lower, yet they remain common. The summed relative
778 abundance of methanotrophic archaeal groups is approximately 4-fold higher in pockmark
779 cores than in adjacent reference cores, averaging $8.3 \pm 12.2\%$ and $2.0 \pm 4.1\%$, respectively.
780 AOM-associated archaea, primarily ANME-2b and, to a lesser extent, ANME-3, are, however,
781 enriched in selected pockmark horizons. Methanogenic archaea are abundant in both pockmark
782 and reference cores, with a moderately higher average summed relative abundance in
783 pockmarks ($18 \pm 11.4\%$) than in references ($14.0 \pm 11.4\%$). However, in pockmark cores, the
784 diversity of methanogenic taxa, and to a lesser extent methanotrophic taxa, is higher
785 (Supplementary material Figs S7, S8).

786

787 Archaeal read abundances were generally higher in pockmark cores than in reference cores,
788 particularly at MET4, where abundances peak in the shallow horizon (Supplementary material
789 Fig. S10). In pockmark cores, archaeal abundances typically peak in the upper to middle parts
790 of the sampled profiles, except in P/MET1-BH, where the trend is reversed (Supplementary
791 material Fig. S10). Similarly, in the reference cores, archaeal abundances peak in the upper to
792 middle horizons, except in the S/MET1-BH core, where abundance increases with depth
793 (Supplementary material Fig. S10).



795

796

797

798

799

800

Fig. 8. Archaeal community composition and multivariate structure in pockmark and reference sediment cores from the south-eastern Baltic Sea. (a) Class-level relative abundance profiles (stacked bars) of archaeal communities in pockmark (P) and reference (S) sediment samples from MET1-BH, MET1-MP, MET3, and MET4. Bars show the proportional contribution of archaeal classes in each sample; sample suffixes indicate depth horizons (as explained in section 2.2). (b) Class-level heatmap of centred

801 log-ratio (CLR)-transformed relative abundances, with hierarchical clustering (dendrograms) of samples
802 and archaeal classes, showing covariation among classes and samples, where red indicates higher
803 relative enrichment and green indicates lower relative enrichment. (c) Multidimensional scaling (MDS)
804 ordination of archaeal community composition shows partial separation between pockmark and
805 reference samples (PERMANOVA, $p = 0.003$). MDS shows significant separation (PERMANOVA, p
806 $= 0.003$), with reference samples more dispersed and pockmark samples more tightly grouped. Taxa
807 driving within-group variability differ between habitats: Hadarchaeia and Halobacteria dominate the
808 pockmark ordination, whereas Methanobacteria, ANME and Hadarchaeia drive the reference ordination.
809 (d) Ordination biplot showing the archaeal classes that contribute most strongly to community variation
810 in pockmark and reference samples, respectively. Nanoarchaeia dominate across all sites. Pockmark
811 horizons show elevated Methanosarcinia (MET1-MP, MET4), whereas reference horizons show
812 stronger contributions from Thermoplasmata and/or Bathyarchaeia. Hierarchical clustering reveals
813 partial intermixing of pockmark and reference samples, indicating that community structure reflects
814 both habitat type and site-specific variability. (e) Family-level heatmap of archaeal relative abundance
815 (CLR-transformed community structure), showing taxonomic groups not visible at the class level, i.e.,
816 ANME-2a-2b.

817

818 **3.6 Correlation network**

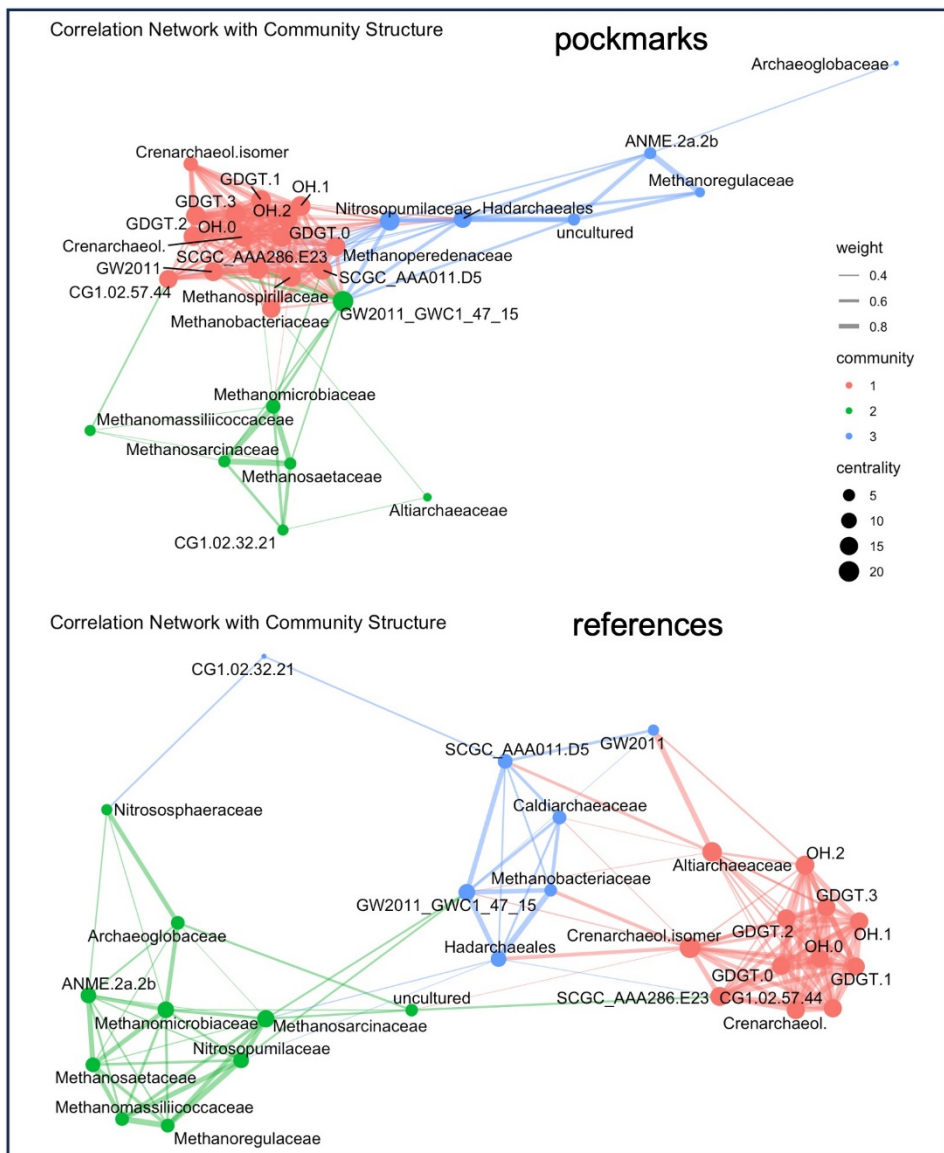
819 To link GDGT patterns to probable biological sources, we combined iGDGT and OH-GDGT
820 abundances with archaeal 16S rRNA relative abundances at the family level using correlation
821 network analysis. This approach identified co-varying lipid–taxon modules that may indicate
822 common sources, ecological niches, or interconnected processes rather than direct biosynthesis
823 alone.

824 In pockmark sediments, the correlation network resolves three main archaeal communities that
825 co-vary (Fig. 9). The first community (red) comprises the full suite of measured GDGTs and is
826 most strongly connected to several Nanoarchaeia lineages (GW2011, SCGC_AAA286_E23,
827 CG1.02.57.44, SCGC_AAA011.D5), with additional links to Methanoperedenaceae. The
828 second community is dominated by ammonia-oxidising Nitrosopumilaceae and clusters with
829 Hadarchaeales. Within this module, Nitrosopumilaceae show the strongest positive associations
830 with GDGT-0, the remaining iGDGTs, and OH-GDGTs. The same module contains ANME-
831 2a-2b, Methanoregulaceae, and uncultured lineages that are strongly interconnected with one
832 another but show comparatively weaker links to GDGTs. Archaeoglobaceae form a peripheral
833 node and does not link to any GDGTs in pockmarks. The third community comprises

834 methanogenic lineages, including Methanospirillaceae, Methanobacteriaceae,
835 Methanosarcinaceae, Methanosaetaceae, Methanomicrobiaceae, Methanomassiliicoccaceae
836 and CG1.02.32.21 (associated with the order Micrarchaeales). These are less directly linked to
837 GDGTs but strongly interlinked with one another. This cluster also includes another
838 representative of Nanoarchaeia (GW2011_GWC1_47_15).

839 In reference sediments, GDGT associations are more broadly distributed across archaeal
840 groups, and the network exhibits higher modularity, with clearer separation among modules. A
841 lipid cluster (crenarchaeol, cren', GDGT-0-3, and OH-GDGTs) correlates with both ammonia
842 oxidisers (Nitrosopumilaceae, Nitrososphaeraceae) and multiple methanogenic families
843 (Methanosaetaceae, Methanosarcinaceae, Methanoregulaceae, Methanomicrobiaceae,
844 Methanomassiliicoccaceae). Compared with pockmarks, methanogens show fewer direct links
845 to the GDGT cluster and more to ANME-2a-2b. Archaeoglobaceae links to Nitrososphaeraceae
846 and methanogens.

847 Overall, the pockmark network exhibits low modularity and relatively dense connectivity,
848 indicating a closely coupled archaeal community. At the same time, the strongest GDGT
849 associations are observed with Nitrosopumilaceae, implying that AOA predominantly influence
850 GDGT co-variation in pockmarks, whereas methanogens/ANME form more distinct sub-
851 clusters characterised by weaker GDGT coupling.



852
 853 Fig. 9. Correlation networks linking archaeal lipid biomarkers and community members in pockmark
 854 and reference (non-pockmark) sediments. Nodes represent lipid variables (GDGTs, OH-GDGTs) and
 855 archaeal taxa (family level). Edge thickness reflects correlation strength; node colour denotes
 856 modules/communities (1–3); node size reflects centrality (larger nodes indicate more central or highly
 857 connected features). Lipid variables form a tightly connected subnetwork (module 1; red), while
 858 additional modules comprise methane-cycling and other archaeal lineages. Module connectivity differs
 859 between pockmark and non-pockmark sites, indicating habitat-dependent coupling between biomarkers
 860 and archaeal taxa. Pockmark networks show tighter coupling between lipid biomarkers and methane-
 861 cycling lineages, whereas reference sediments display clearer module separation, with lipids and the
 862 archaeal community varying more independently.

863
 864
 865

866 **4 Discussion**

867 **4.1 Archaeal community structure in methane-influenced pockmark sediment cores**

868

869 The archaeal community structure and porewater profiles of CH₄ and SO₄²⁻ indicate that the
870 investigated pockmarks are CH₄-influenced yet spatially heterogeneous sedimentary systems.
871 At the microbial community level, pockmark cores are not characterised by a complete
872 replacement of the archaeal groups inhabiting reference sediments, but rather by localised
873 enrichment of CH₄-cycling lineages. This is most evident at lower taxonomic levels, where
874 ANME-2b (genus-level distribution; supplementary material Fig. S7a,b), ANME-2a-2b,
875 Methanosarcinaceae, Methanosacetaceae, Methanomicrobiaceae (family-level distribution; Fig.
876 8e; supplementary material Fig. S6), and other CH₄-associated taxa are enriched in selected
877 pockmark horizons. Pockmark cores exhibit substantially higher methanogen diversity (11
878 genera detected) and a higher abundance of CH₄-cycling archaea (approximately 3-fold) than
879 reference cores (6 genera) (Supplementary material, Fig. S7a,b). Correspondingly, total iGDGT
880 and OH-GDGT concentrations are approximately three times higher in pockmark cores than in
881 reference cores (Fig. 4, 8). In the correlation network (Fig. 9), pockmarks represent a tightly
882 coupled metabolic system in which various archaeal groups act in concert — likely CH₄-
883 impacted — whereas at the reference sites these groups form less integrated sub-communities,
884 with stronger representation of ammonia-oxidising *Ca. Nitrosopumilus* (Supplementary
885 material Fig. S7a,b), heterotrophic Thermoplasmata associated with acidic, sulphur-rich
886 environments (González-Toril et al., 2006), and organic matter-degrading Bathyarchaeia (Zhou
887 et al., 2018). This suggests that in reference cores, microorganisms have more independent
888 ecological roles, which could be explained by higher sulphate concentration and lower methane
889 concentration (Fig. 2). On the other hand, the summed relative abundances of methanotrophic
890 archaea are approximately 4-fold higher in pockmark cores than in reference cores, whereas
891 methanogens are moderately more abundant in pockmark cores than in reference cores. This
892 suggests that AOM-associated lineages are more closely linked to pockmark niches, whereas
893 methanogenic taxa occupy broader anoxic sedimentary niches of the studied basin. The Gdańsk
894 Basin is characterised by high organic matter loading resulting from eutrophication (Łukawska-
895 Matuszewska et al., 2014), yet eutrophication and methanogenesis is widespread in the oxygen-
896 and sulphate-depleted Baltic Sea (Schmale et al., 2010 with references therein; Carstensen et
897 al., 2014; Lapham et al., 2024). However, the Baltic Sea exhibits considerable microbial
898 diversity (Ininbergs et al., 2015), due to eutrophication and pollution, steep horizontal and

899 vertical gradients in salinity and nutrient levels, the presence of freshwater and marine phyla,
900 as well as autochthonous brackish populations.

901

902 **4.2 Methanogenic archaea and depth-related community shifts**

903 The absolute abundance of methanogens in pockmarks increases with sediment depth, except
904 for the mid-depth of P/MET4, which harbours an excessive abundance of *Methanosarcina*.
905 *Methanosarcina* predominates across all sediment horizons in both pockmark and reference
906 cores (Supplementary material Fig. S8), likely owing to its metabolic versatility (Sowers et al.,
907 1993; Galagan et al., 2002; Maeder et al., 2006), which confers competitive advantages under
908 fluctuating environmental conditions (e.g., hydrostatic pressure governing freshened porewater
909 seepage, seasonal thermocline dynamics, nutrient and organic matter availability, North Sea
910 saline water inflow). The vertical distribution of methanogenic archaea varies with sediment
911 depth (Supplementary material, Fig. S8), whereas *Methanosarcina* and *Methanosaeta*
912 predominantly populate the examined sediment horizons, except in the reference cores S/MET3
913 and S/MET4, which are dominated by *Methanosarcina*, and some of the bottom samples are
914 dominated by *Methanoregula*. Both *Methanosarcina* and *Methanosaeta* drive acetoclastic
915 methanogenesis (Conklin et al., 2006; Welte et al., 2014) and are favoured in sediments rich in
916 labile organic matter (Li et al., 2022). Both are also major contributors to the GDGT-0 pool in
917 estuarine sediments (De Rosa et al., 1977; Schouten et al., 2013; Bauersachs et al., 2015). At
918 the same time, GDGT-0 is the second most abundant GDGT in the analysed samples after
919 crenarchaeol (Fig. 5). The remaining major components of the methanogenic community that
920 appear to alternate – sometimes with *Methanosaeta*, sometimes with SDB – are *Methanoregula*
921 and *Methanogenium*, exhibiting a downcore shift.

922 Interestingly, a distinct dominance shift appears in the reference cores S/MET3 and S/MET4,
923 where *Methanosaeta* is replaced by *Methanosarcina* (Supplementary material, Fig. S8), which
924 may indicate the onset of an environmental stressor, such as shifts in oxygen, ammonium, or
925 organic matter concentrations that influence pH (De Vrieze, 2014). This shift coincides with a
926 high relative abundance of *Ca. Nitrosopumilus*, *Ca. Aenigmarchaeum*, and *Woesearchaeales*
927 (AR15, AR20) (Supplementary material, Fig. S7a); however, the communities in the references
928 S/MET3 and S/MET4 split into distinct groups, with surface AOA-DPANN-rich and
929 subsurface different archaeal groups (Fig. 8b). In corresponding pockmark cores, *Methanosaeta*
930 abundance declines remarkably in P/MET3 (especially in the uppermost sediment horizon) and

931 in P/MET4 (especially in the lowermost horizon) and is replaced by diverse hydrogenotrophic
932 genera, belonging to the Methanobacteria and Methanomicrobia class, including
933 *Methanogenium*, *Methanospirillum*, *Methanomicrobium*, *Methanoculleus*,
934 *Methanocorpusculum*, *Methanobrevibacter*, *Methanolinea*, *Methanoregula*, and SDB, which
935 may indicate a seasonal shift towards hypoxic/anoxic conditions in bottom water and high
936 organic matter degradation/supply. This methanogenic community shift coincides with elevated
937 CH₄ concentrations in the pockmarks P/MET3 and P/MET4 (Fig. 2). Adam-Beyer et al. (2025)
938 directly link the presence and activity of *Methanogenium* in the incubation experiment on
939 sediments collected in the South-Western Baltic Sea to phytoplankton blooms and a high supply
940 of organic matter, resulting in organic matter degradation and oxygen depletion, which catalyse
941 methanogenesis. In light of these findings, Kapustina et al. (2026) reported, at the time our
942 samples were collected in October 2019, relatively high oxygen levels above the halocline (60-
943 70 m) and hypoxic conditions below it (70-100 m), with permanent euxinia in the deep layers
944 of the Gdańsk Deep (100 m and deeper). The contribution of hydrogenotrophic methanogens
945 increases as the transition from freshened porewater-influenced pockmarks in the MET1 area
946 of the Gulf of Gdańsk (mostly inferred from previous studies and discussed below in Section
947 4.3; supplementary material, Fig. S1) to marine conditions in the Gdańsk Deep is observed (i.e.,
948 higher sulphate concentrations, Fig. 2). The BIT index indicates a marine organic matter source
949 with very low terrestrial input across both pockmark and reference cores; interestingly, the
950 mean values increase along the Gulf of Gdańsk-Gdańsk Deep transect (Table 1; supplementary
951 material, Fig. S3).

952 Pockmark core P/MET4 exhibits the highest total GDGT concentrations and the most
953 pronounced individual GDGT peaks (Fig. 4; supplementary material Fig. S4), whilst the second
954 highest concentrations are observed in pockmark core P/MET3. The above-mentioned
955 hydrogenotrophic Methanomicrobia are known to produce acyclic GDGTs (Bale et al., 2019;
956 Zeng et al., 2022), and among Methanobacteria, genus *Methanobrevibacter* is an identified
957 GDGT-0 producer (Bauersachs et al., 2015; Elling et al., 2017). However, in terms of relative
958 abundance, *Methanosarcinia* and *Methanosaeta* in pockmarks are 1.25–1.65 times more
959 abundant than hydrogenotrophic methanogens and 1–26.25 times more abundant than in
960 references. Similar hydrogenotrophic communities have been documented in an inactive
961 pockmark within the Hanko Basin, northern Baltic Sea (Purkamo et al., 2022). In this dataset,
962 pockmark P/MET3 was inactive during the study period and showed no porewater freshening,

963 whereas pockmark P/MET4 is characterised by weak seabed activity (Supplementary material
964 Fig. S1, Table S1).

965 **4.3 Porewater geochemistry, SMI development**

966 Porewater profiles of CH₄ and SO₄²⁻ show stronger CH₄ accumulation and sharper SO₄²⁻
967 depletion, particularly at MET1-MP, MET1-BH, and MET4, indicating active or recent
968 methane supply and shallow sulphate-methane interface (from 5 to ~15 cm bsf) where CH₄ and
969 SO₄²⁻ gradients overlap (Fig. 2). In marine sediments, elevated seawater sulphate concentrations
970 primarily limit microbial methane production to deeper sediment layers below the sulphatic
971 zone (Jørgensen, 2021). However, in the studied pockmarks and reference sites of the MET1
972 area affected by porewater freshening, low sulphate concentrations below ca. 25 cm of sediment
973 depth promote microbial methane production. Freshened groundwater seepage in the MET1
974 area, first reported by Idczak et al. (2020), Brodecka-Goluch et al. (2022), and Rzepa et al.
975 (2026), significantly affects the microbial community by altering the chemical environment,
976 leading to sulphate depletion in porewater and promoting methanogenesis throughout the entire
977 sediment column rather than just in deeper layers. This was demonstrated by the dominance of
978 Methanomicrobia during the freshwater outflow episode and of Nanoarchaeia during the
979 saltwater intrusion episode. Although in pockmark P/MET3 porewater freshening has not been
980 observed and the Cl⁻ concentrations are similar to those of the reference core (Fig. 2), next to
981 freshened porewater influence, sulphate depletion may be caused by high organic loading,
982 where microbial demand for electron acceptors is high and sulphate is consumed rapidly. This
983 typically occurs in the top metre of sediment below the seafloor in the Baltic Sea (Zinke et al.,
984 2019).

985 Previously, it was suggested that freshened groundwater seepage dilutes the already low
986 chloride and sulphate concentrations in the pockmarks MET1-BH and MET1-MP (Brodecka-
987 Goluch et al., 2022; Idczak et al., 2020; Łukawska-Matuszewska and Dwornik, 2025). Chloride
988 profiles in pockmarks MET1 and MET4 show lower Cl⁻ concentrations than adjacent reference
989 cores (Fig. 2), suggesting that freshened porewater discharge may be diluting SO₄²⁻ (Fig. 2),
990 thereby influencing both the depth and the archaeal community structure of the methane
991 oxidation zone. Kurowski et al. (2024) analysed the MET1-BH pockmark and suggested that
992 iron-dependent anaerobic oxidation of methane (Fe-AOM) serves as an alternative pathway
993 when sulphate is limited in the MET1 area. The reduced SO₄²⁻ availability in porewaters of
994 CH₄-rich Baltic Sea sediments appears to shift the microbial community towards utilising iron

995 (oxyhydr)oxides as alternative oxidants for AOM (Egger et al., 2017). These iron
996 (oxyhydr)oxides are common in the Gulf of Gdańsk (Kurowski et al., 2024). As indicated by
997 higher concentrations of dissolved Fe^{2+} and Mn^{2+} and increased precipitation of authigenic
998 carbonates, AOM in the MET1 area may be coupled to iron reduction (Rzepa et al., 2026).
999 Furthermore, in northern Baltic Sea pockmarks, SGD-driven advection compresses redox and
1000 reaction zones, reduces organic matter accumulation, suppresses SMI development, and leads
1001 to archaeal communities dominated by AOA, whereas diffusion-dominated inactive pockmarks
1002 accumulate organic-rich sediments characterised by a prevalence of methanogens (Purkamo et
1003 al., 2022).

1004 P/MET1-BH shows strong CH_4 enrichment and SO_4^{2-} depletion, indicating an active or recently
1005 active methane-influenced redox zone (Fig. 2). However, its GDGT concentrations are much
1006 lower than those in pockmarks P/MET3 and P/MET4. Conversely, P/MET3 shows substantial
1007 GDGT accumulation despite weaker porewater methane enrichment and a less pronounced
1008 archaeal presence involved in CH_4 cycling. This decoupling suggests that the bulk GDGT pool
1009 integrates in situ archaeal production, contributions from sedimentary lineages such as
1010 Methanomicrobia, Methanosarcinia, Thermoplasmata, and possibly others and uncultivated
1011 archaea, together with pelagic input of Nitrososphaeria-derived crenarchaeol.

1012 In pockmark P/MET4, the strongest porewater methane enrichment coincides with
1013 exceptionally high relative abundance of Methanosarcinaceae (Fig. 2, 8e) and below the SMI,
1014 with exceptionally high relative abundance of ANME-2a-2b (and ANME-2b at the genus level)
1015 (Fig. 8e; supplementary material Figs. S6, S7a,b) and high sulphate concentration (Fig. 2),
1016 which indicates rather high productivity of this pockmark. At the same time, for the S/MET4
1017 reference site, the low methane concentration of 0.011 mM is the highest throughout the profile
1018 and sulphate concentration remains high; however, the bottom-most sample of the archaeal
1019 community shows 0 reads (Fig. 8a), while in the upper part of the profile dominates uncultured
1020 lineages and Nanoarchaeia. Pockmark MET1-MP also shows pronounced enrichment of
1021 ANME-2a-2b at the deeper part of the profile below SMI (and ANME-2b at the genus level)
1022 (Fig. 8e; supplementary material Figs. S6, S7a, b), and in the reference core, at the mid-depth
1023 of the profile below the shallow SMI, which may suggest deeper ANME zonation.. Thus,
1024 methane-related communities are not limited to the pockmark core but extend into adjacent
1025 sediments. However, reference cores S/MET3 and S/MET4 do not show methanotrophic
1026 archaea (Supplementary material, Fig. S9), which aligns with the low/absent CH_4 (Fig. 2).

1027 Ultimately, groundwater discharge influences microbial community composition by
1028 transporting microorganisms within sediments; however, prevailing environmental conditions
1029 and interactions determine which microorganisms become dominant (Justice et al., 2017).

1030 **4.4 Controls on archaeal lipid accumulation: methane cycling, LOI, and pockmark** 1031 **activity**

1032 The iGDGT distribution profiles offer an additional lipid-based perspective on the spatial
1033 heterogeneity of the investigated pockmark systems. Pockmark cores, particularly P/MET3 and
1034 P/MET4, show elevated concentrations of archaeal lipids \sum iGDGT and \sum OH-GDGT (Figs. 4,
1035 6) relative to adjacent reference cores, indicating enhanced archaeal lipid accumulation in
1036 selected pockmark cores. In the pockmark core P/MET4, high iGDGT concentrations coincide
1037 with strong porewater CH₄ enrichment, SO₄²⁻ depletion (Fig. 2), lower Cl⁻ concentrations
1038 relative to the reference core (Fig. 2), and local enrichment of methane-cycling archaea (Fig.
1039 8e), including ANME-2b, ANME-3, and methanogen-affiliated genera (Supplementary
1040 material Figs. S6a, b, S7, S8). Taken together, these suggest that CH₄ cycling and possibly weak
1041 porewater freshening contributed to the archaeal lipid signal. The elevated GDGT-3
1042 concentration in pockmark P/MET4 is also consistent with a locally increased contribution from
1043 ANME-3 (at P/MET4/5; supplementary material Fig. S7a), although GDGT-3 is not source-
1044 specific.

1045 To assess whether elevated \sum iGDGT concentrations might simply reflect higher bulk organic
1046 matter content, GDGT profiles were compared with LOI-derived trends in organic matter (full-
1047 core elemental TOC data were not available for all sites) (Supplementary material Fig. S2). LOI
1048 was used as a screening-level proxy, supported by comparisons of measured TOC and LOI
1049 profiles in representative cores, which show comparable vertical trends (Supplementary
1050 material Fig. S2). The use of LOI as an organic matter proxy is supported by previous regional
1051 geochemical research by Łukawska-Matuszewska et al. (2014), based on a substantially larger
1052 sample set, which demonstrated a strong correlation ($R^2=0.68$) between LOI and organic carbon.
1053 The findings indicate that LOI is an effective screening tool for assessing geochemical
1054 variability related to organic matter.

1055 This comparison indicates that \sum iGDGT and \sum OH-GDGT concentrations are not tightly
1056 coupled to bulk organic matter (Figs 3-4, 6; supplementary material Fig. S2). In several cores,
1057 GDGT profiles do not align with LOI trends: for example, pockmark P/MET1-BH shows

1058 relatively high LOI and clear CH₄ enrichment with SO₄²⁻ depletion, yet does not exhibit the
1059 strongest GDGT accumulation, whereas pockmark P/MET3 contains elevated \sum iGDGT and
1060 \sum OH-GDGT concentrations despite weaker porewater CH₄ enrichment and a smaller
1061 contribution from methane-cycling archaea than P/MET4. The strong GDGT enrichment
1062 cannot be fully explained by elevated LOI across pockmark profiles, because the tetraether lipid
1063 maxima do not align with those of bulk organic matter. However, due to limitations of the LOI
1064 application, such as sensitivity to experimental conditions, interference from sediment
1065 composition, and loss of inorganic carbon, TOC measurements should be performed on the
1066 samples to verify the relationship between organic matter content and tetraether lipids.

1067 Lipid preservation could potentially be a side effect of the less ebullitive nature of methane
1068 seepage in pockmarks P/MET3 and P/MET4, thereby enhancing CH₄ accumulation over time:
1069 the kinetics and episodicity of CH₄ supply to the seabed and of freshened porewater discharge
1070 are reduced in pockmarks P/MET3 and P/MET4 compared with those reported in previous
1071 studies (Idczak et al., 2020; Brodecka-Goluch et al., 2022; Łukawska-Matuszewska and
1072 Dwornik, 2025; Rzepa et al., 2026) for more hydrologically complex pockmarks of the MET1
1073 area. Additionally, present-day dissolved CH₄ and SO₄²⁻ profiles may not fully capture the
1074 temporal geochemical variability of this environment. As reported by Treude et al. (2005), the
1075 spatial and temporal heterogeneity caused by gas ebullition allows methanogens and sulphate
1076 reducers to coexist in Eckernförde Bay, feeding the shallow SMI, but also enables CH₄ to
1077 escape into the overlying water column, bypassing the microbial barrier.

1078 **4.5 Limitations of GDGT-based AOM proxies in ANME-2/ANME-3-dominated** 1079 **pockmarks of the Gdańsk Basin**

1080 Peaks in archaeal abundance (Supplementary material Fig. S10) and in GDGT concentrations
1081 at sediment depths of 5–45 cm could mark the SMI (Fig. 2). However, iGDGTs indices (Table
1082 1; supplementary material Fig. S3) do not support a strong AOM imprint, as values remain
1083 uniformly low. MI values (<0.09) fall well below the 0.3-0.5 threshold indicative of CH₄-
1084 impacted sediments observed by Zhang et al. (2011). However, for the MI value to reach 0.5,
1085 methanotrophic-derived GDGT must constitute approximately 30-50% of the total GDGT pool
1086 (Kim and Zhang, 2023).

1087 A low MI index, calculated as the ratio of GDGT-1-3 to crenarchaeol, typically indicates
1088 minimal methanotrophic contribution relative to Nitrososphaeria-derived sources (Zhang et al.,

1089 2011). The uniformly low MI values observed here likely reflect a strong crenarchaeol signal
1090 from ammonia-oxidising archaea thriving above, in the water column and/or limited GDGT-1-
1091 3 production by the dominant AOM lineages, rather than definitively excluding AOM. GDGT-
1092 1 to -3, which increase substantially in ANME-1-dominated systems (Rossel et al., 2008), are
1093 two orders of magnitude less abundant in the analysed samples than GDGT-0 and crenarchaeol,
1094 consistent with the near-absence of ANME-1 (maximum relative abundance of 0.6% in
1095 S/MET3/5; Fig. 8a).

1096 Although the applicability of MI to ANME-2 and ANME-3 (which dominate the AOM
1097 community here; supplementary material Fig. S8) has been questioned, comprehensive
1098 biomarker investigations generally support its utility for AOM detection (Kim and Zhang,
1099 2023). Nevertheless, ANME-2 and ANME-3 alone are unlikely to contribute substantially to
1100 GDGT production (Niemann and Elvert, 2008; Weijers et al., 2011), making MI non-diagnostic
1101 in this study. The consistently low GDGT-2/cren ratios (maximum 0.04; Table 1) support this
1102 interpretation. This ratio typically indicates CH₄-rich AOM conditions, under which ANME-1-
1103 synthesised GDGT-2 (Rossel et al., 2008) is elevated relative to crenarchaeol. To further
1104 evaluate the GDGT distribution characteristics of an AOM-related SMI, the relative abundances
1105 of GDGT-1, GDGT-2, and GDGT-3 were compared across cores. In contrast to the GDGT-2-
1106 dominated pattern reported by Weijers et al. (2011), GDGT-2 was not the dominant compound
1107 in any of our samples. Instead, 74 of 75 samples showed the order GDGT-1 > GDGT-2 >
1108 GDGT-3. This indicates that the investigated cores do not show enrichment of GDGT-2,
1109 consistent with uniformly low GDGT-2/crenarchaeol ratios.

1110 Nevertheless, ANME lineages are more prevalent in pockmark cores (Supplementary material
1111 Fig. S9), suggesting, relatively to reference cores, enhanced AOM activity, particularly at
1112 P/MET3 and P/MET4. Peaks in GDGT-1 to -3 concentrations also occur in reference cores,
1113 following the general trend for all iGDGTs, but at lower concentrations (Supplementary
1114 material Fig. S4). In addition, certain core GDGTs (e.g., GDGT-1) may arise from diagenetic
1115 and degradative processes acting on phosphohexose headgroups predominantly produced by
1116 *Ca. Nitrosopumilus* in the Baltic Sea (Wittenborn et al., 2023).

1117 Overall, AOM activity appears shallow within the studied pockmarks, consistent with previous
1118 investigations demonstrating weak S-AOM confined to thin, shallow sediment layers and
1119 potentially dependent on alternative electron acceptors in deeper layers (Broclawik et al., 2020;
1120 Idczak et al., 2020; Brodecka-Goluch et al., 2022; Łukawska-Matuszewska et al., 2022; Ehlert

1121 von Ahn et al., 2024). The minor contribution of *Ca. Methanoperedens* in the dataset (MET1-
1122 MP; supplementary material Fig. S9) indicates traces of AOM coupled to nitrate and/or metal
1123 oxide reduction. Members of the family Methanoperedenaceae (formerly ANME-2D) typically
1124 inhabit sulphate-depleted freshwater systems and perform AOM independently of syntrophic
1125 partnerships (Haroon et al., 2013; Ettwig et al., 2016; Vaksmaa et al., 2017; Leu et al., 2020).

1126 **4.6 Methanogens and GDGT-based proxies**

1127 Within the CH₄-cycling archaeal community, methanogens appear to be the primary
1128 contributors to GDGT biosynthesis (Fig. 5). Although GDGT-0 and crenarchaeol predominate
1129 in marine sediments (Schouten et al., 2002), their elevated concentrations across all investigated
1130 gas systems indicate that they serve as primary iGDGT biomarkers in the sediments of the
1131 Gdańsk Basin, even in CH₄-rich settings harbouring both methanogenic and methanotrophic
1132 communities. However, GDGT-0 lacks source specificity and can be synthesised by multiple
1133 archaeal lineages, including methanogens and methanotrophs (Pancost et al., 2001; Blaga et al.,
1134 2009; Inglis et al., 2015; Słowakiewicz et al., 2016; Petrick et al., 2019). These lineages may
1135 also produce cyclised GDGTs (Koga et al., 1993; Weijers et al., 2006; Schouten et al., 2013;
1136 Bauersachs et al., 2015), although this is not always replicable in culture studies (Bauersachs et
1137 al., 2015).

1138 The network analysis indicates that AOA-associated crenarchaeol and the statistically co-
1139 varying GDGT-0 are the primary drivers of variation in the bulk GDGT pool (Fig. 9), likely
1140 masking the methanogen signal by influencing the GDGT-0/cren ratio through crenarchaeol
1141 contribution from pelagic Nitrososphaeria. The observed GDGT-0/cren ratios in Gdańsk Basin
1142 samples are <0.99, well below the 2 threshold characteristic of methanogen-dominated systems
1143 (Schouten et al., 2002; Blaga et al., 2009), indicating minimal methanogen contribution and
1144 AOA predominance. In the northern Baltic Sea pockmarks (Hanko Basin), Nitrososphaeria –
1145 including some groundwater-origin populations – constitute a major component of the archaeal
1146 community (Purkamo et al., 2022), consistent with evidence that *Ca. Nitrosopumilus* is a
1147 widespread, important GDGT-producing lineage in the Baltic Sea (Wittenborn et al., 2023).
1148 However, sedimentary iGDGTs integrate archaeal lipid production and export over longer
1149 timescales, and their distribution is further shaped by preservation conditions (Lengger et al.,
1150 2013), while in contrast, amplicon-based relative abundance reflects the compositional
1151 distribution of recovered 16S rRNA gene reads after DNA extraction (Gloor et al., 2017) and
1152 does not directly indicate lipid production rates.

1153 **4.7 AOA and non-methane archaeal lipid sources**

1154 Given that AOA are abundant in the Baltic Sea under low-oxygen conditions and along redox
1155 gradients (Berg et al., 2015b), GDGT-0/cren ratios (<1) and very high abundance of *Ca.*
1156 *Nitrosopumilus* in both pockmark and reference sediment cores (Supplementary material, Fig.
1157 S7), suggest a substantial contribution of crenarchaeol most likely originating from the water
1158 column. Although our samples do not represent the archaeal community in the source
1159 groundwater and were collected during a single season, the groundwater-associated
1160 Nitrososphaeria reported by Purkamo et al. (2022), such as *Nitrosoarchaeum* or *Ca.*
1161 *Nitrosotalea*, were not identified. Instead, Nitrososphaeria is represented only by *Ca.*
1162 *Nitrosopumilus*, a major AOA taxon in the Baltic Sea water column (Wittenborn et al., 2023
1163 with references therein), therefore supporting pelagic AOA origin of crenarchaeol in the studied
1164 samples.

1165 Methane seepage creates chemically reducing conditions that limit the growth of oxygen-
1166 dependent organisms. However, AOA can persist and function (Jakobs et al., 2016) in sharp
1167 chemical gradients and microenvironments (e.g., thin oxic/suboxic boundary layers). Martens-
1168 Habbena and Qin (2022) showed that *Nitrosopumilus maritimus* can sustain ammonia oxidation
1169 under oxygen-depleted conditions, further indicating that AOA may be flexible and
1170 physiologically adapted to redox-variable conditions.

1171 Nevertheless, elevated summed iGDGT and OH-GDGT concentrations in pockmarks P/MET3
1172 and P/MET4 (especially GDGT-0 and crenarchaeol; Figs. 4–7) may indicate an indirect
1173 ecological linkage between the nitrogen and carbon biogeochemical cycles in the studied
1174 system, in which sulphate reduction, degradation of organic matter, methanogenesis, and other
1175 anaerobic processes release NH_4^+ and other reduced compounds into porewaters. These
1176 compounds may subsequently be transported (diffused) into the bottom waters and the
1177 overlying water column, where Nitrososphaeria thrive. Consequently, crenarchaeol remains the
1178 dominant iGDGT in both pockmark and reference cores (Supplementary material Fig. S4), as
1179 Nitrososphaeria is abundant in the overlying water column and may feed on the products of
1180 enhanced processes occurring in the sediments.

1181 Thus, intensified organic matter degradation may influence GDGT accumulation, as evidenced
1182 by the GDGT profiles of pockmarks P/MET3 and P/MET4 in the Gdańsk Deep, which are
1183 characterised by historically documented weak or absent seabed activity (Supplementary

1184 material Fig. S1, Table S1), in contrast to the seabed activity observed at pockmark MET1. To
1185 better investigate organic matter degradation in the studied pockmarks, porewater alkalinity and
1186 ammonia concentrations should be measured concurrently with GDGTs. However, the
1187 particularly high Σ iGDGT and Σ OH-GDGT concentrations in pockmark P/MET4 coincide with
1188 the highest porewater concentrations of CH_4 and SO_4^{2-} and with the most abundant and diverse
1189 CH_4 -cycling archaeal community among the sites examined. This may imply elevated primary
1190 productivity and the deposition of organic matter that settles on the seafloor, which fuels
1191 decomposition and methanogenesis in the sediments, but also indicates thriving conditions for
1192 Thaumarchaeota in the water column. Despite the AOA dominance recorded in crenarchaeol
1193 concentration and very high relative abundance of *Ca. Nitrosopumilus* (Supplementary material
1194 Fig. S7), GDGT-0 concentrations remain relatively elevated across the pockmark sites,
1195 particularly at the inactive pockmark P/MET3 and the weakly active pockmark P/MET4, which
1196 experiences weak, occasional porewater seepage, compared with active venting systems
1197 characterised by focused CH_4 flow, such as mud volcanoes on the Canadian Beaufort Sea slope
1198 (Lee et al., 2018) and studied here pockmarks MET1-MP and MET1-BH (Supplementary
1199 material Fig. S4).

1200 Average OH-GDGT% values align with those reported for Baltic Sea surface sediments
1201 (Sinninghe Damsté et al., 2022), and RI-OH and RI-OH' values are within the Baltic/Skagerrak
1202 Surface sediment ranges (Sinninghe Damsté et al., 2022). While salinity primarily controls OH-
1203 GDGT behaviour (Sinninghe Damsté et al., 2022), recent studies show strong responses to
1204 nitrate availability and water-column stratification (Harning and Sepúlveda, 2024), indicating
1205 an ecological influence on RI-OH/RI-OH'. The most robust interpretation is that OH-GDGTs
1206 primarily track AOA, particularly Nitrososphaeria, as supported by culture studies (Sinninghe
1207 Damsté et al., 2022). In our data, OH-GDGTs closely covary with crenarchaeol, consistent with
1208 previous findings indicating thaumarchaeotal source (Kaiser and Arz, 2016).

1209 Furthermore, Nanoarchaeota, prevalent across the samples, may be involved in ectosymbiosis
1210 with Nitrososphaeria, consistent with their reliance on symbiotic relationships (Waters et al.,
1211 2003). Nanoarchaeota may also possess GDGTs, previously attributed to their biological hosts
1212 (Zeng et al., 2022), which could explain their correlation with GDGTs (Fig. 9). They can also
1213 associate with methanogens (Brick et al., 2025), which may explain their high relative
1214 abundance (~40% in non-pockmark and ~55% in pockmark sediments). Other frequent groups,
1215 e.g., AR15 and AR20, are likewise symbiotic or parasitic; the latter, linked to groundwater

1216 (Castelle et al., 2015), could underscore the influence of porewater freshening in the Gulf of
1217 Gdańsk in pockmarks MET1-MP and MET1-BH.

1218 Several archaeal groups, including Thermoplasmata, Bathyarchaeia, Lokiarchaeia,
1219 Heimdallarchaeia, Archaeoglobi, and the Deep Sea Euryarchaeotic Group (DSEG; within
1220 Thermoplasmata; Rinke et al., 2021), are associated with the degradation of complex organic
1221 matter, aromatic carbon degradation, protein catabolism, and fermentation (Zinke et al., 2019).
1222 These groups — particularly Bathyarchaeia and Thermoplasmata — are more abundant in
1223 reference cores than in pockmarks and may contribute to GDGT production in anoxic
1224 environments (Besseling et al., 2018, 2020; Baxter et al., 2021). Bathyarchaeia thrive in anoxic
1225 environments, degrading recalcitrant organic matter (Baxter and Zalar, 2019; Blewett et al.,
1226 2022; Zeng et al., 2022), whereas Archaeoglobi mediate both sulphate reduction and
1227 methanogenesis (Lynes et al., 2024). Bathyarchaeia may also occupy a central position in
1228 archaeal carbon-nitrogen networks, co-occurring with methanogens and Nitrososphaeria, and
1229 potentially linking organic carbon degradation with reduced nitrogen availability (Yi et al.,
1230 2024). However, despite the abundance of Bathyarchaeia and Nitrososphaeria in the archaeal
1231 community structure, this mechanism remains inferential, as NH_4^+ and AOA activity were not
1232 directly measured herein. Asgard archaea, including hydrocarbon-degrading Lokiarchaeia and
1233 hydrogen-dependent acetogenic Heimdallarchaeia (Zhang et al., 2025), also show higher
1234 abundance in reference cores and may contribute to iGDGT production, likely GDGT-0 (Zeng
1235 et al., 2022). Although the tetraether synthase (Tes) gene, essential for GDGT biosynthesis, has
1236 been identified in Hadarchaeia and Altiarchaeia, GDGTs have not yet been detected in these
1237 groups (Zeng et al., 2022). Notably, some Hadarchaeia grow syntrophically with methanogens
1238 (Yu et al., 2024). Interestingly, Thermococci which is known to produce GDGT-0 (Zeng et al.,
1239 2022), has not been resolved at lower taxonomic levels in our samples, but shows high
1240 abundance in pockmarks (Fig. 8a).

1241 **5. Conclusions**

1242 This study presents the first integrated analysis of archaeal 16S rRNA communities,
1243 sedimentary iGDGT/OH-GDGT distributions, and microbial correlation networks in methane
1244 pockmarks of the Gdańsk Basin. Pockmarks host more diverse and abundant archaeal
1245 communities than adjacent reference sites, and due to correlation network, function as tightly
1246 coupled metabolic systems, whereas reference sites exhibit more niche-partitioned ecological
1247 structures. Despite CH_4 -rich conditions, evidence for AOM remains limited. Low MI values

1248 and the near absence of ANME-1 reduce the reliability of GDGT-based AOM proxies in studied
1249 settings. Low GDGT-0/cren and GDGT-2/cren ratios indicate dominance of pelagic AOA,
1250 particularly *Ca. Nitrosopumilus*, which may mask methanogenic GDGT signals, but do not
1251 support a groundwater origin for Nitrososphaeria in the studied gas systems, as hypothesised
1252 for pockmarks in Hanko Bay, Baltic Sea. However, the dominance of GDGT-0 and
1253 crenarchaeol in specific pockmarks may reveal intricate linkages between microbial community
1254 structure (i.e., Bathyarchaeia and Nitrososphaeria) and the underlying biogeochemical
1255 processes. The transport of reduced compounds from anaerobic reactions across the sediment-
1256 water interface may enhance the proliferation of Nitrososphaeria.

1257 The mixing of freshened groundwater with marine porewater, together with gas seepage, may
1258 indicate localised microbial “hotspots” with higher archaeal diversity. Our findings show that
1259 pockmarks in the Gdańsk Basin can act as spatially heterogeneous and temporally variable
1260 hotspots of archaeal activity, with community composition reflecting the intensity of the
1261 methane-cycling reaction zone, which develops where local geochemical gradients favour
1262 methanogenesis and AOM, irrespective of whether seabed gas escape is strongly expressed at
1263 the time of observation. Differences between active (P/MET1) and inactive (P/MET3) or
1264 weakly active (P/MET4) pockmarks are reflected in archaea abundance, methane-cycling
1265 archaeal community structure, and Σ iGDGT concentrations, but the relationship is non-linear.
1266 Pockmark P/MET4 shows a strong CH₄-cycling archaeal signal despite being only weakly
1267 active at the seabed, which can indicate the importance of subsurface conditions for methane
1268 production, as well as for the accumulation, decomposition, and mineralisation of organic
1269 matter; while active pockmark MET1-BH may lose CH₄ through periodic, strong, and focused
1270 gas and water seepage and potential gas escape.

1271 Our study defines the conditions and limitations under which iGDGTs can be interpreted in
1272 Baltic Sea pockmarks. Local CH₄-driven processes do not fundamentally alter the sedimentary
1273 tetraether lipid record, which instead reflects the broader marine environmental signal. The
1274 clearest combined biomarker, geochemical, and microbiological evidence for methane cycling,
1275 observed mostly at pockmark P/MET4, indicates increased iGDGT concentrations, elevated
1276 CH₄, depleted SO₄²⁻, and shallow SMI, along with enrichment of ANME-2b, ANME-3,
1277 hydrogenotrophic methanogens, and where *Methanosarcina*, *Methanosaeta*, and
1278 *Methanoregula* co-occur. However, the iGDGT distribution in the weakly active pockmark
1279 P/MET4 is similar to that of the adjacent reference sediments, probably indicating a pelagic

1280 AOA source. The inactive pockmark P/MET3 also shows increased accumulation of archaeal
1281 tetraether lipids compared with the reference core. As in pockmark P/MET4, the iGDGT
1282 distribution is primarily associated with water-column processes of pelagic AOA rather than
1283 with processes driven by CH₄-cycling communities in the sediment, as evidenced by the
1284 dominance of crenarchaeol. Active MET1 pockmarks also show iGDGT distributions similar
1285 to those of adjacent reference cores, so the differences between pockmarks lie in the
1286 concentration of iGDGTs rather than in their distribution. Therefore, the concentration profiles
1287 of iGDGT and OH-GDGT could perhaps serve as a proxy for primary productivity in the Baltic
1288 Sea.

1289 Future studies should integrate GDGT analyses with methane-specific biomarkers (e.g.,
1290 crocetane, PMI, archaeol, hydroxyarchaeol), NH₄⁺ concentrations, porewater alkalinity,
1291 compound-specific carbon isotopes, and functional gene or transcriptomic approaches (e.g.,
1292 *mcrA*) to better constrain active CH₄ cycling and identify the responsible ANME clades, as well
1293 as spatial activity of Nitrososphaeria. Measuring both core and intact polar lipids in sediments
1294 and the water column would further clarify GDGT production, transport, and preservation.
1295 Overall, this study highlights the need for integrated multi-proxy and multi-omic approaches to
1296 distinguish active microbial processes from preserved diagenetic signals in methane seep
1297 systems influenced by submarine groundwater discharge, porewater freshening, and dynamic
1298 redox conditions.

1299

1300 *Data availability.* All iGDGT data is available in the repository 10.5281/zenodo.18414700.

1301 *Author contributions.* IDMS and MS designed the research; IDMS evaluated the geochemical
1302 and microbiological data; AB, ABG, and KLM collected the samples; AB prepared the
1303 microbiological dataset; IDMS and AB conducted the statistical analyses; IDMS wrote the
1304 manuscript; FP and MS reviewed and edited the manuscript.

1305 *Competing interests.* The contact author has declared that none of the authors has any
1306 competing interests.

1307 *Acknowledgements.* This study was partially funded by the Elsevier Research Scholarship
1308 (awarded to IDMS). IDMS is grateful to the Organic Geochemistry Group at Utrecht University
1309 for assistance with analyses. AB, ABG, and KLM thank the captain and crew of RV *Oceanograf*

1310 for their support during the cruises. Paweł Działak is thanked for isolating material for DNA
1311 analysis. We are also grateful to the handling editor and two anonymous reviewers for their
1312 detailed and helpful comments.

1313

1314 **References**

- 1315 Adam-Beyer, N., Deusner, C., Schmidt, M., and Perner, M.: Microbial hydrogen oxidation
1316 potential in seasonally hypoxic Baltic Sea sediments, *Frontiers in Microbiology*, 16,
1317 <https://doi.org/10.3389/fmicb.2025.1565157>, 2025.
- 1318 Aitchison, J.: The statistical analysis of compositional data, *Journal of the Royal Statistical*
1319 *Society: Series B (Methodological)*, 44, 139–160, [https://doi.org/10.1111/j.2517-](https://doi.org/10.1111/j.2517-6161.1982.tb01195.x)
1320 [6161.1982.tb01195.x](https://doi.org/10.1111/j.2517-6161.1982.tb01195.x), 1982.
- 1321 Bale, N. J., Palatinszky, M., Rijpstra, W. I. C., Herbold, C. W., Wagner, M., and Sinninghe
1322 Damsté, J. S.: Membrane lipid composition of the moderately thermophilic ammonia-
1323 oxidizing archaeon “*Candidatus Nitrosotenuis uzonensis*” at different growth temperatures,
1324 *Applied and Environmental Microbiology*, 85, e01332-19,
1325 <https://doi.org/10.1128/AEM.01332-19>, 2019.
- 1326 Bauersachs, T., Weidenbach, K., Schmitz, R. A., and Schwark, L.: Distribution of glycerol
1327 ether lipids in halophilic, methanogenic and hyperthermophilic archaea, *Organic*
1328 *Geochemistry*, 83–84, 101–108, <https://doi.org/10.1016/j.orggeochem.2015.03.009>, 2015.
- 1329 Baxter, A. J., van Bree, L. G. J., Peterse, F., Hopmans, E. C., Villanueva, L., Verschuren, D.,
1330 and Sinninghe Damsté, J. S.: Seasonal and multi-annual variation in the abundance of
1331 isoprenoid GDGT membrane lipids and their producers in the water column of a meromictic
1332 equatorial crater lake (Lake Chala, East Africa), *Quaternary Science Reviews*, 273, 107263,
1333 <https://doi.org/10.1016/j.quascirev.2021.107263>, 2021.
- 1334 Baxter, B. K. and Zalar, P.: The extremophiles of Great Salt Lake: Complex microbiology in
1335 a dynamic hypersaline ecosystem, in: *Model Ecosystems in Extreme Environments*, edited by:
1336 Seckbach, J. and Rampelotto, P., Academic Press, 57–99, [https://doi.org/10.1016/B978-0-12-](https://doi.org/10.1016/B978-0-12-812742-1.00004-0)
1337 [812742-1.00004-0](https://doi.org/10.1016/B978-0-12-812742-1.00004-0), 2019.
- 1338 Berg, C., Listmann, L., Vandieken, V., Vogts, A., and Jürgens, K.: Chemoautotrophic growth
1339 of ammonia-oxidizing Thaumarchaeota enriched from a pelagic redox gradient in the Baltic
1340 Sea, *Frontiers in Microbiology*, 5, <https://doi.org/10.3389/fmicb.2014.00786>, 2015a.
- 1341 Berg, C., Vandieken, V., Thamdrup, B., and Jürgens, K.: Significance of archaeal nitrification
1342 in hypoxic waters of the Baltic Sea, *The ISME Journal*, 9, 1319–1332,
1343 <https://doi.org/10.1038/ismej.2014.218>, 2015b.
- 1344 Besseling, M. A., Hopmans, E. C., Boschman, R. C., Sinninghe Damsté, J. S., and
1345 Villanueva, L.: Benthic archaea as potential sources of tetraether membrane lipids in
1346 sediments across an oxygen minimum zone, *Biogeosciences*, 15, 4047–4064,
1347 <https://doi.org/10.5194/bg-15-4047-2018>, 2018.

- 1348 Besseling, M. A., Hopmans, E. C., Bale, N. J., Schouten, S., Damsté, J. S. S., and Villanueva,
 1349 L.: The absence of intact polar lipid-derived GDGTs in marine waters dominated by Marine
 1350 Group II: Implications for lipid biosynthesis in Archaea, *Scientific Reports*, 10, 294,
 1351 <https://doi.org/10.1038/s41598-019-57035-0>, 2020.
- 1352 Bijl, P. K., Śliwińska, K. K., Duncan, B., Huguet, A., Naeher, S., Rattanasriampaipong, R.,
 1353 Sosa-Montes de Oca, C., Auderset, A., Berke, M. A., Kim, B. S., Davtian, N., Dunkley Jones,
 1354 T., Eefting, D. D., Elling, F. J., Fenies, P., Inglis, G. N., O'Connor, L., Pancost, R. D.,
 1355 Peterse, F., Rice, A., Sluijs, A., Varma, D., Xiao, W., and Zhang, Y. G.: Reviews and
 1356 syntheses: Best practices for the application of marine GDGTs as proxy for
 1357 paleotemperatures: sampling, processing, analyses, interpretation, and archiving protocols,
 1358 *Biogeosciences*, 22, 6465–6508, <https://doi.org/10.5194/bg-22-6465-2025>, 2025.
- 1359 Blaga, C. I., Reichart, G.-J., Heiri, O., and Sinninghe Damsté, J. S.: Tetraether membrane
 1360 lipid distributions in water-column particulate matter and sediments: a study of 47 European
 1361 lakes along a north–south transect, *Journal of Paleolimnology*, 41, 523–540,
 1362 <https://doi.org/10.1007/s10933-008-9242-2>, 2009.
- 1363 Blainey, P. C., Mosier, A. C., Potanina, A., Francis, C. A., and Quake, S. R.: Genome of a
 1364 low-salinity ammonia-oxidizing archaeon determined by single-cell and metagenomic
 1365 analysis, *PLoS One*, 6, e16626, <https://doi.org/10.1371/journal.pone.0016626>, 2011.
- 1366 Blewett, J., Elling, F. J., Naafs, B. D. A., Kattein, L., Evans, T. W., Lauretano, V., Gallego-
 1367 Sala, A. V., Pancost, R. D., and Pearson, A.: Metabolic and ecological controls on the stable
 1368 carbon isotopic composition of archaeal (isoGDGT and BDGT) and bacterial (brGDGT)
 1369 lipids in wetlands and lignites, *Geochimica et Cosmochimica Acta*, 320, 1–25,
 1370 <https://doi.org/10.1016/j.gca.2021.12.023>, 2022.
- 1371 Blondel, V. D., Guillaume, J.-L., Lambiotte, R., and Lefebvre, E.: Fast unfolding of
 1372 communities in large networks, *Journal of Statistical Mechanics: Theory and Experiment*,
 1373 2008, P10008, <https://doi.org/10.1088/1742-5468/2008/10/P10008>, 2008.
- 1374 Boetius, A., Ravensschlag, K., Schubert, C. J., Rickert, D., Widdel, F., Gieseke, A., Amann,
 1375 R., Jørgensen, B. B., Witte, U., and Pfannkuche, O.: A marine microbial consortium
 1376 apparently mediating anaerobic oxidation of methane, *Nature*, 407, 623–626,
 1377 <https://doi.org/10.1038/35036572>, 2000.
- 1378 van den Boogaart, K. G., Tolosana-Delgado, R., and Bren, M.: Package “compositions”:
 1379 Compositional Data Analysis, 2024.
- 1380 Brick, S., Niggemann, J., Reckhardt, A., Könneke, M., and Engelen, B.: Interstitial microbial
 1381 communities of coastal sediments are dominated by Nanoarchaeota, *Frontiers in*
 1382 *Microbiology*, 16, 1532193, <https://doi.org/10.3389/fmicb.2025.1532193>, 2025.
- 1383 Broclawik, O., Łukawska-Matuszewska, K., Brodecka-Goluch, A., and Bolalek, J.: Impact of
 1384 methane occurrence on iron speciation in the sediments of the Gdansk Basin (Southern Baltic
 1385 Sea), *Science of The Total Environment*, 721, 137718,
 1386 <https://doi.org/10.1016/j.scitotenv.2020.137718>, 2020.
- 1387 Brodecka, A., Majewski, P., Bolalek, J., and Klusek, Z.: Geochemical and acoustic evidence
 1388 for the occurrence of methane in sediments of the Polish sector of the southern Baltic Sea*,
 1389 *Oceanologia*, 55, 951–978, <https://doi.org/10.5697/oc.55-4.951>, 2013.

- 1390 Brodecka-Goluch, A., Idczak, J., Gorska, N., and Bolałek, J.: Geophysical and geochemical
1391 characteristics of four different pockmark sites located in the Gdańsk Basin, in: *Earth system*
1392 *changes and Baltic Sea coasts*, 89–90, 2020.
- 1393 Brodecka-Goluch, A., Łukawska-Matuszewska, K., Kotarba, M. J., Borkowski, A., Idczak, J.,
1394 and Bolałek, J.: Biogeochemistry of three different shallow gas systems in continental shelf
1395 sediments of the South-Eastern Baltic Sea (Gulf of Gdańsk): Carbon cycling, origin of
1396 methane and microbial community composition, *Chemical Geology*, 597, 120799,
1397 <https://doi.org/10.1016/j.chemgeo.2022.120799>, 2022.
- 1398 Burnett, W. C., Bokuniewicz, H., Huettel, M., Moore, W. S., and Taniguchi, M.: Groundwater
1399 and pore water inputs to the coastal zone, *Biogeochemistry*, 66, 3–33,
1400 <https://doi.org/10.1023/B:BIOG.0000006066.21240.53>, 2003.
- 1401 Burnett, W. C., Aggarwal, P. K., Aureli, A., Bokuniewicz, H., Cable, J. E., Charette, M. A.,
1402 Kontar, E., Krupa, S., Kulkarni, K. M., Loveless, A., Moore, W. S., Oberdorfer, J. A.,
1403 Oliveira, J., Ozyurt, N., Povinec, P., Privitera, A. M. G., Rajar, R., Ramessur, R. T., Scholten,
1404 J., Stieglitz, T., Taniguchi, M., and Turner, J. V.: Quantifying submarine groundwater
1405 discharge in the coastal zone via multiple methods, *Science of The Total Environment*, 367,
1406 498–543, <https://doi.org/10.1016/j.scitotenv.2006.05.009>, 2006.
- 1407 Bussmann, I. and Suess, E.: Groundwater seepage in Eckernförde Bay (Western Baltic Sea):
1408 Effect on methane and salinity distribution of the water column, *Continental Shelf Research*,
1409 18, 1795–1806, [https://doi.org/10.1016/S0278-4343\(98\)00058-2](https://doi.org/10.1016/S0278-4343(98)00058-2), 1998.
- 1410 Callow, B., Bull, J. M., Provenzano, G., Böttner, C., Birinci, H., Robinson, A. H., Henstock,
1411 T. J., Minshull, T. A., Bayrakci, G., Lichtschlag, A., Roche, B., Yilo, N., Gehrman, R.,
1412 Karstens, J., Falcon-Suarez, I. H., and Berndt, C.: Seismic chimney characterisation in the
1413 North Sea – Implications for pockmark formation and shallow gas migration, *Marine and*
1414 *Petroleum Geology*, 133, 105301, <https://doi.org/10.1016/j.marpetgeo.2021.105301>, 2021.
- 1415 Carman, R. and Jonsson, P.: Distribution patterns of different forms of phosphorus in some
1416 surficial sediments of the Baltic Sea, *Chemical Geology*, 90, 91–106,
1417 [https://doi.org/10.1016/0009-2541\(91\)90036-Q](https://doi.org/10.1016/0009-2541(91)90036-Q), 1991.
- 1418 Carstensen, J., Conley, D. J., Bonsdorff, E., Gustafsson, B. G., Hietanen, S., Janas, U., Jilbert,
1419 T., Maximov, A., Norkko, A., Norkko, J., Reed, D. C., Slomp, C. P., Timmermann, K., and
1420 Voss, M.: Hypoxia in the Baltic Sea: biogeochemical cycles, benthic fauna, and management,
1421 *AMBIO*, 43, 26–36, <https://doi.org/10.1007/s13280-013-0474-7>, 2014.
- 1422 Castelle, C. J., Wrighton, K. C., Thomas, B. C., Hug, L. A., Brown, C. T., Wilkins, M. J.,
1423 Frischkorn, K. R., Tringe, S. G., Singh, A., Markillie, L. M., Taylor, R. C., Williams, K. H.,
1424 and Banfield, J. F.: Genomic expansion of domain Archaea highlights roles for organisms
1425 from new phyla in anaerobic carbon cycling, *Current Biology*, 25, 690–701,
1426 <https://doi.org/10.1016/j.cub.2015.01.014>, 2015.
- 1427 Chen, S., Zhou, Y., Chen, Y., and Gu, J.: fastp: an ultra-fast all-in-one FASTQ preprocessor,
1428 *Bioinformatics*, 34, i884–i890, <https://doi.org/10.1093/bioinformatics/bty560>, 2018.
- 1429 Conklin, A., Stensel, H. D., and Ferguson, J.: Growth kinetics and competition between
1430 *Methanosarcina* and *Methanosaeta* in mesophilic anaerobic digestion, *Water Environment*
1431 *Research*, 78, 486–496, <https://doi.org/10.2175/106143006X95393>, 2006.

- 1432 De Rosa, M., De Rosa, S., Gambacorta, A., Minale, L., and Bu'lock, J. D.: Chemical structure
1433 of the ether lipids of thermophilic acidophilic bacteria of the Caldariella group,
1434 *Phytochemistry*, 16, 1961–1965, [https://doi.org/10.1016/0031-9422\(77\)80105-2](https://doi.org/10.1016/0031-9422(77)80105-2), 1977.
- 1435 De Vrieze, J.: *Methanosaeta vs. Methanosarcina in anaerobic digestion: the quest for*
1436 *enhanced biogas production*, dissertation, Ghent University, 2014.
- 1437 Dearing Crampton-Flood, E., Peterse, F., and Sinninghe Damsté, J. S.: Production of
1438 branched tetraethers in the marine realm: Svalbard fjord sediments revisited, *Organic*
1439 *Geochemistry*, 138, 103907, <https://doi.org/10.1016/j.orggeochem.2019.103907>, 2019.
- 1440 Díaz-Mendoza, G. A., Krämer, K., von Rönn, G. A., Schwarzer, K., Heinrich, C., Reimers,
1441 H.-C., and Winter, C.: Circular structures on the seabed: differentiating between natural and
1442 anthropogenic origins—Examples from the Southwestern Baltic Sea, *Frontiers in Earth*
1443 *Science*, 11, 1170787, 2023.
- 1444 Ding, S., Kohlhepp, B., Trumbore, S., Küsel, K., Totsche, K.-U., Pohnert, G., Gleixner, G.,
1445 and Schwab, V. F.: In situ production of core and intact bacterial and archaeal tetraether lipids
1446 in groundwater, *Organic Geochemistry*, 126, 1–12,
1447 <https://doi.org/10.1016/j.orggeochem.2018.10.005>, 2018.
- 1448 Egger, M., Hagens, M., Sapart, C. J., Dijkstra, N., van Helmond, N. A. G. M., Mogollón, J.
1449 M., Risgaard-Petersen, N., van der Veen, C., Kasten, S., Riedinger, N., Böttcher, M. E.,
1450 Röckmann, T., Jørgensen, B. B., and Slomp, C. P.: Iron oxide reduction in methane-rich deep
1451 Baltic Sea sediments, *Geochimica et Cosmochimica Acta*, 207, 256–276,
1452 <https://doi.org/10.1016/j.gca.2017.03.019>, 2017.
- 1453 Ehlert von Ahn, C. M., Dellwig, O., Szymczycha, B., Kotwicki, L., Rooze, J., Endler, R.,
1454 Escher, P., Schmiedinger, I., Sültenfuß, J., Diak, M., Gehre, M., Struck, U., Vogler, S., and
1455 Böttcher, M. E.: Submarine groundwater discharge into a semi-enclosed coastal bay of the
1456 southern Baltic Sea: A multi-method approach, *Oceanologia*, 66, 111–138,
1457 <https://doi.org/10.1016/j.oceano.2024.01.001>, 2024.
- 1458 Elling, F. J., Könneke, M., Nicol, G. W., Stieglmeier, M., Bayer, B., Spieck, E., de la Torre, J.
1459 R., Becker, K. W., Thomm, M., Prosser, J. I., Herndl, G. J., Schleper, C., and Hinrichs, K.-U.:
1460 Chemotaxonomic characterisation of the thaumarchaeal lipidome, *Environmental*
1461 *Microbiology*, 19, 2681–2700, <https://doi.org/10.1111/1462-2920.13759>, 2017.
- 1462 Engvall, A.-G.: *The fate of nitrogen in early diagenesis of Baltic sediments: a study of the*
1463 *sediment-water interface*, PhD thesis, University of Stockholm, Stockholm, 16 pp., 1978.
- 1464 Ettwig, K. F., Zhu, B., Speth, D., Keltjens, J. T., Jetten, M. S. M., and Kartal, B.: Archaea
1465 catalyze iron-dependent anaerobic oxidation of methane, *Proceedings of the National*
1466 *Academy of Sciences*, 113, 12792–12796, <https://doi.org/10.1073/pnas.1609534113>, 2016.
- 1467 Fenies, P., Ho, S. L., Hefter, J., and Lee, P.-T.: Impact of anaerobic methanotrophic archaeal
1468 input on hydroxylated isoprenoid GDGT-derived temperatures, *Organic Geochemistry*, 218,
1469 105213, <https://doi.org/10.1016/j.orggeochem.2026.105213>, 2026.
- 1470 Galagan, J. E., Nusbaum, C., Roy, A., Endrizzi, M. G., Macdonald, P., FitzHugh, W., Calvo,
1471 S., Engels, R., Smirnov, S., Atnoor, D., Brown, A., Allen, N., Naylor, J., Stange-Thomann,
1472 N., DeArellano, K., Johnson, R., Linton, L., McEwan, P., McKernan, K., Talamas, J., Tirrell,

- 1473 A., Ye, W., Zimmer, A., Barber, R. D., Cann, I., Graham, D. E., Grahame, D. A., Guss, A.
1474 M., Hedderich, R., Ingram-Smith, C., Kuettner, H. C., Krzycki, J. A., Leigh, J. A., Li, W.,
1475 Liu, J., Mukhopadhyay, B., Reeve, J. N., Smith, K., Springer, T. A., Umayam, L. A., White,
1476 O., White, R. H., Conway de Macario, E., Ferry, J. G., Jarrell, K. F., Jing, H., Macario, A. J.
1477 L., Paulsen, I., Pritchett, M., Sowers, K. R., Swanson, R. V., Zinder, S. H., Lander, E.,
1478 Metcalf, W. W., and Birren, B.: The genome of *M. acetivorans* reveals extensive metabolic
1479 and physiological diversity, *Genome Research*, 12, 532–542,
1480 <https://doi.org/10.1101/gr.223902>, 2002.
- 1481 Gloor, G. B., Macklaim, J. M., Pawlowsky-Glahn, V., and Egozcue, J. J.: Microbiome
1482 datasets are compositional: and this is not optional, *Frontiers in Microbiology*, 8, 2224, 2017.
- 1483 González-Toril, E., Gómez, F., Malki, M., and Amils, R.: The isolation and study of
1484 Acidophilic microorganisms, in: *Methods in Microbiology*, vol. 35, Academic Press, 471–
1485 510, [https://doi.org/10.1016/S0580-9517\(08\)70023-0](https://doi.org/10.1016/S0580-9517(08)70023-0), 2006.
- 1486 Guan, H., Liu, L., Birgel, D., Peckmann, J., Feng, D., and Li, S.: Hydroxylated GDGTs-0 in
1487 marine methane seep environments: A putative indicator for archaeal methanogenesis,
1488 *Organic Geochemistry*, 198, 104862, <https://doi.org/10.1016/j.orggeochem.2024.104862>,
1489 2024.
- 1490 Haroon, M. F., Hu, S., Shi, Y., Imelfort, M., Keller, J., Hugenholtz, P., Yuan, Z., and Tyson,
1491 G. W.: Anaerobic oxidation of methane coupled to nitrate reduction in a novel archaeal
1492 lineage, *Nature*, 500, 567–570, <https://doi.org/10.1038/nature12375>, 2013.
- 1493 Hedges, J. I. and Stern, J. H.: Carbon and nitrogen determinations of carbonate-containing
1494 solids¹, *Limnology and Oceanography*, 29, 657–663,
1495 <https://doi.org/10.4319/lo.1984.29.3.0657>, 1984.
- 1496 Hoffmann, J. J. L., Schneider von Deimling, J., Schröder, J. F., Schmidt, M., Held, P.,
1497 Crutchley, G. J., Scholten, J., and Gorman, A. R.: Complex eyed pockmarks and submarine
1498 groundwater discharge revealed by acoustic data and sediment cores in Eckernförde Bay, SW
1499 Baltic Sea, *Geochemistry, Geophysics, Geosystems*, 21, e2019GC008825,
1500 <https://doi.org/10.1029/2019GC008825>, 2020.
- 1501 Hopmans, E. C., Schouten, S., and Sinninghe Damsté, J. S.: The effect of improved
1502 chromatography on GDGT-based palaeoproxies, *Organic Geochemistry*, 93, 1–6,
1503 <https://doi.org/10.1016/j.orggeochem.2015.12.006>, 2016.
- 1504 Hovland, M. and Judd, A. G.: *Seabed Pockmarks and Seepages. Impact on Geology, Biology
1505 and the Marine Environment*, Graham & Trotman (Kluwer), London, Dordrecht, Boston, 293
1506 pp., 1988.
- 1507 Hovland, M., Gardner, J. V., and Judd, A. G.: The significance of pockmarks to
1508 understanding fluid flow processes and geohazards, *Geofluids*, 2, 127–136, 2002.
- 1509 Huguet, A., Fosse, C., Laggoun-Défarge, F., Toussaint, M.-L., and Derenne, S.: Occurrence
1510 and distribution of glycerol dialkyl glycerol tetraethers in a French peat bog, *Organic
1511 Geochemistry*, 41, 559–572, <https://doi.org/10.1016/j.orggeochem.2010.02.015>, 2010.
- 1512 Huguet, C., Hopmans, E. C., Febo-Ayala, W., Thompson, D. H., Sinninghe Damsté, J. S., and
1513 Schouten, S.: An improved method to determine the absolute abundance of glycerol

- 1514 dibiphytanyl glycerol tetraether lipids, *Organic Geochemistry*, 37, 1036–1041,
1515 <https://doi.org/10.1016/j.orggeochem.2006.05.008>, 2006.
- 1516 Huguet, C., Fietz, S., and Rosell-Melé, A.: Global distribution patterns of hydroxy glycerol
1517 dialkyl glycerol tetraethers, *Organic Geochemistry*, 57, 107–118,
1518 <https://doi.org/10.1016/j.orggeochem.2013.01.010>, 2013.
- 1519 Idczak, J., Brodecka-Goluch, A., Łukawska-Matuszewska, K., Graca, B., Gorska, N., Klusek,
1520 Z., Pezacki, P. D., and Bolałek, J.: A geophysical, geochemical and microbiological study of a
1521 newly discovered pockmark with active gas seepage and submarine groundwater discharge
1522 (MET1-BH, central Gulf of Gdańsk, southern Baltic Sea), *Science of The Total Environment*,
1523 742, 140306, <https://doi.org/10.1016/j.scitotenv.2020.140306>, 2020.
- 1524 Inglis, G. N., Farnsworth, A., Lunt, D., Foster, G. L., Hollis, C. J., Pagani, M., Jardine, P. E.,
1525 Pearson, P. N., Markwick, P., Galsworthy, A. M. J., Raynham, L., Taylor, Kyle. W. R., and
1526 Pancost, R. D.: Descent toward the Icehouse: Eocene sea surface cooling inferred from
1527 GDGT distributions, *Paleoceanography*, 30, 1000–1020,
1528 <https://doi.org/10.1002/2014PA002723>, 2015.
- 1529 Ininbergs, K., Bergman, B., Larsson, J., and Ekman, M.: Microbial metagenomics in the
1530 Baltic Sea: Recent advancements and prospects for environmental monitoring, *AMBIO*, 44,
1531 439–450, <https://doi.org/10.1007/s13280-015-0663-7>, 2015.
- 1532 Jakobs, G., Labrenz, M., Rehder, G., Hietanen, S., Kießlich, K., Vogts, A., Blumenberg, M.,
1533 and Schmale, O.: A boreactor approach to investigate the linkage between methane oxidation
1534 and nitrate/nitrite reduction in the pelagic oxic-anoxic transition zone of the Central Baltic
1535 Sea, *Frontiers in Marine Science*, 3, <https://doi.org/10.3389/fmars.2016.00145>, 2016.
- 1536 Jakobsson, M., O'Regan, M., Mörth, C.-M., Stranne, C., Weidner, E., Hansson, J.,
1537 Gyllencreutz, R., Humborg, C., Elfving, T., Norkko, A., Norkko, J., Nilsson, B., and
1538 Sjöström, A.: Potential links between Baltic Sea submarine terraces and groundwater seeping,
1539 *Earth Surface Dynamics*, 8, 1–15, <https://doi.org/10.5194/esurf-8-1-2020>, 2020.
- 1540 Jäntti, H., Ward, B. B., Dippner, J. W., and Hietanen, S.: Nitrification and the ammonia-
1541 oxidizing communities in the central Baltic Sea water column, *Estuarine, Coastal and Shelf
1542 Science*, 202, 280–289, <https://doi.org/10.1016/j.ecss.2018.01.019>, 2018.
- 1543 Jaśniewicz, D., Klusek, Z., Brodecka-Goluch, A., and Bolałek, J.: Acoustic investigations of
1544 shallow gas in the southern Baltic Sea (Polish Exclusive Economic Zone): a review, *Geo-
1545 Marine Letters*, 39, 1–17, <https://doi.org/10.1007/s00367-018-0555-5>, 2019.
- 1546 Jaworowski, K., Wagner, R., Modliski, Z., Pokorski, J., Sokołowski, J., and Sokołowski, A.:
1547 Marine ecogeology in semi-closed basin: case study on a threat of geogenic pollution of the
1548 southern Baltic Sea (Polish Exclusive Economic Zone), *Geological Quarterly*, 54, 267–288,
1549 2010.
- 1550 Jensen, J. B., Kuijpers, A., Bennike, O., Laier, T., and Werner, F.: New geological aspects for
1551 freshwater seepage and formation in Eckernförde Bay, western Baltic, *Continental Shelf
1552 Research*, 22, 2159–2173, [https://doi.org/10.1016/S0278-4343\(02\)00076-6](https://doi.org/10.1016/S0278-4343(02)00076-6), 2002.
- 1553 Jørgensen, B. B.: Sulfur biogeochemical cycle of marine sediments, *Geochemical
1554 Perspectives*, 10, 145–146, 2021.

- 1555 Jørgensen, B. B., Weber, A., and Zopfi, J.: Sulfate reduction and anaerobic methane oxidation
1556 in Black Sea sediments, *Deep Sea Research Part I: Oceanographic Research Papers*, 48,
1557 2097–2120, [https://doi.org/10.1016/S0967-0637\(01\)00007-3](https://doi.org/10.1016/S0967-0637(01)00007-3), 2001.
- 1558 Justice, N. B., Sczesnak, A., Hazen, T. C., and Arkin, A. P.: Environmental selection,
1559 dispersal, and organism interactions shape community assembly in high-throughput
1560 enrichment culturing, *Applied and Environmental Microbiology*, 83, e01253-17,
1561 <https://doi.org/10.1128/AEM.01253-17>, 2017.
- 1562 Kaiser, J. and Arz, H. W.: Sources of sedimentary biomarkers and proxies with potential
1563 paleoenvironmental significance for the Baltic Sea, *Continental Shelf Research*, 122, 102–
1564 119, <https://doi.org/10.1016/j.csr.2016.03.020>, 2016.
- 1565 Kapustina, M., Bubnova, E., and Dudkov, I.: Deep water of the Gdansk Deep (Baltic Sea):
1566 variability of hydrology and dissolved oxygen over recent decades, *Regional Studies in*
1567 *Marine Science*, 93, 104727, <https://doi.org/10.1016/j.rsma.2025.104727>, 2026.
- 1568 Kim, B. and Zhang, Y. G.: Methane Index: Towards a quantitative archaeal lipid biomarker
1569 proxy for reconstructing marine sedimentary methane fluxes, *Geochimica et Cosmochimica*
1570 *Acta*, 354, 74–87, <https://doi.org/10.1016/j.gca.2023.06.008>, 2023.
- 1571 King, L. H. and MacLean, B.: Pockmarks on the Scotian Shelf, *GSA Bulletin*, 81, 3141–3148,
1572 1970.
- 1573 Knittel, K. and Boetius, A.: Anaerobic oxidation of methane: progress with an unknown
1574 process, *Annual Review of Microbiology*, 63, 311–334,
1575 <https://doi.org/10.1146/annurev.micro.61.080706.093130>, 2009.
- 1576 Koga, Y., Nishihara, M., Morii, H., and Akagawa-Matsushita, M.: Ether polar lipids of
1577 methanogenic bacteria: structures, comparative aspects, and biosyntheses, *Microbiological*
1578 *Reviews*, 57, 164–182, <https://doi.org/10.1128/mr.57.1.164-182.1993>, 1993.
- 1579 Kotarba, M. J.: Origin of hydrocarbon gases accumulated in the Middle Cambrian reservoirs
1580 of the Polish part of the Baltic region, *Geological Quarterly*, 54, 197–204, 2010.
- 1581 Kotarba, M. J. and Lewan, M. D.: Sources of natural gases in Middle Cambrian reservoirs in
1582 Polish and Lithuanian Baltic Basin as determined by stable isotopes and hydrous pyrolysis of
1583 Lower Palaeozoic source rocks, *Chemical Geology*, 345, 62–76,
1584 <https://doi.org/10.1016/j.chemgeo.2013.02.023>, 2013.
- 1585 Kotarba, M. J. and Nagao, K.: Molecular and isotopic compositions and origin of natural
1586 gases from Cambrian and Carboniferous-Lower Permian reservoirs of the onshore Polish
1587 Baltic region, *International Journal of Earth Sciences*, 104, 241–261,
1588 <https://doi.org/10.1007/s00531-014-1063-0>, 2015.
- 1589 Kreuzburg, M., Scholten, J., Hsu, F.-H., Liebetrau, V., Sültenfuß, J., Rapaglia, J., and
1590 Schlüter, M.: Submarine groundwater discharge-derived nutrient fluxes in Eckernförde Bay
1591 (Western Baltic Sea), *Estuaries and Coasts*, 46, 1190–1207, [https://doi.org/10.1007/s12237-](https://doi.org/10.1007/s12237-023-01202-0)
1592 [023-01202-0](https://doi.org/10.1007/s12237-023-01202-0), 2023.
- 1593 Kuliński, K., Rehder, G., Asmala, E., Bartosova, A., Carstensen, J., Gustafsson, B., Hall, P.
1594 O. J., Humborg, C., Jilbert, T., Jürgens, K., Meier, H. E. M., Müller-Karulis, B., Naumann,

- 1595 M., Olesen, J. E., Savchuk, O., Schramm, A., Slomp, C. P., Sofiev, M., Sobek, A.,
1596 Szymczycha, B., and Undeman, E.: Biogeochemical functioning of the Baltic Sea, *Earth*
1597 *System Dynamics*, 13, 633–685, <https://doi.org/10.5194/esd-13-633-2022>, 2022.
- 1598 Kurowski, S., Łukawska-Matuszewska, K., Čović, A., Jozić, D., and Brodecka-Goluch, A.:
1599 Effects of pockmark activity on iron cycling and mineral composition in continental shelf
1600 sediments (southern Baltic Sea), *Biogeochemistry*, 167, 135–154,
1601 <https://doi.org/10.1007/s10533-024-01127-1>, 2024.
- 1602 Labrenz, M., Sintes, E., Toetzke, F., Zumsteg, A., Herndl, G. J., Seidler, M., and Jürgens, K.:
1603 Relevance of a crenarchaeotal subcluster related to *Candidatus Nitrosopumilus maritimus* to
1604 ammonia oxidation in the suboxic zone of the central Baltic Sea, *The ISME Journal*, 4, 1496–
1605 1508, <https://doi.org/10.1038/ismej.2010.78>, 2010.
- 1606 Lapham, L. L., Lloyd, K. G., Fossing, H., Flury, S., Jensen, J. B., Alperin, M. J., Rehder, G.,
1607 Holzhueter, W., Ferdelman, T., and Jørgensen, B. B.: Methane leakage through the sulfate–
1608 methane transition zone of the Baltic seabed, *Nature Geoscience*, 17, 1277–1283,
1609 <https://doi.org/10.1038/s41561-024-01594-z>, 2024.
- 1610 Lawal, M. A., Cook, A. E., Portnov, A., and Kumar, A.: Pockmarks, mud volcanoes and
1611 hydrocarbon seeps in the Northern Gulf of Mexico: trends and controls on widespread fluid
1612 and gas venting, *Basin Research*, 38, e70095, <https://doi.org/10.1111/bre.70095>, 2026.
- 1613 Lee, D.-H., Kim, J.-H., Lee, Y. M., Stadnitskaia, A., Jin, Y. K., Niemann, H., Kim, Y.-G., and
1614 Shin, K.-H.: Biogeochemical evidence of anaerobic methane oxidation on active submarine
1615 mud volcanoes on the continental slope of the Canadian Beaufort Sea, *Biogeosciences*, 15,
1616 7419–7433, <https://doi.org/10.5194/bg-15-7419-2018>, 2018.
- 1617 Lengger, S. K., Kraaij, M., Tjallingii, R., Baas, M., Stuut, J.-B., Hopmans, E. C., Sinnighe
1618 Damsté, J. S., and Schouten, S.: Differential degradation of intact polar and core glycerol
1619 dialkyl glycerol tetraether lipids upon post-depositional oxidation, *Organic Geochemistry*, 65,
1620 83–93, <https://doi.org/10.1016/j.orggeochem.2013.10.004>, 2013.
- 1621 Leu, A. O., Cai, C., McIlroy, S. J., Southam, G., Orphan, V. J., Yuan, Z., Hu, S., and Tyson,
1622 G. W.: Anaerobic methane oxidation coupled to manganese reduction by members of the
1623 *Methanoperedenaceae*, *The ISME Journal*, 14, 1030–1041, <https://doi.org/10.1038/s41396-020-0590-x>, 2020.
- 1625 Li, X., Li, Y., Gao, D., Liu, M., and Hou, L.: Methane production linked to organic matter
1626 molecule and methanogenic community in estuarine benthic sediments, *Journal of*
1627 *Geophysical Research: Biogeosciences*, 127, e2022JG007236,
1628 <https://doi.org/10.1029/2022JG007236>, 2022.
- 1629 Liu, Q., Charette, M. A., Breier, C. F., Henderson, P. B., McCorkle, D. C., Martin, W., and
1630 Dai, M.: Carbonate system biogeochemistry in a subterranean estuary – Waquoit Bay, USA,
1631 *Geochimica et Cosmochimica Acta*, 203, 422–439, <https://doi.org/10.1016/j.gca.2017.01.041>,
1632 2017.
- 1633 Liu, X.-L., Summons, R. E., and Hinrichs, K.-U.: Extending the known range of glycerol
1634 ether lipids in the environment: structural assignments based on tandem mass spectral
1635 fragmentation patterns, *Rapid Communications in Mass Spectrometry*, 26, 2295–2302,
1636 <https://doi.org/10.1002/rcm.6355>, 2012.

- 1637 Lu, J., Breitwieser, F. P., Thielen, P., and Salzberg, S. L.: Bracken: estimating species
1638 abundance in metagenomics data, *PeerJ Computer Science*, 3, e104,
1639 <https://doi.org/10.7717/peerj-cs.104>, 2017.
- 1640 Lu, J., Rincon, N., Wood, D. E., Breitwieser, F. P., Pockrandt, C., Langmead, B., Salzberg, S.
1641 L., and Steinegger, M.: Metagenome analysis using the Kraken software suite, *Nature*
1642 *Protocols*, 17, 2815–2839, <https://doi.org/10.1038/s41596-022-00738-y>, 2022.
- 1643 Lü, X., Liu, X.-L., Elling, F. J., Yang, H., Xie, S., Song, J., Li, X., Yuan, H., Li, N., and
1644 Hinrichs, K.-U.: Hydroxylated isoprenoid GDGTs in Chinese coastal seas and their potential
1645 as a paleotemperature proxy for mid-to-low latitude marginal seas, *Organic Geochemistry*,
1646 89–90, 31–43, <https://doi.org/10.1016/j.orggeochem.2015.10.004>, 2015.
- 1647 Lukawska-Matuszewska, K.: Contribution of non-carbonate inorganic and organic alkalinity
1648 to total measured alkalinity in pore waters in marine sediments (Gulf of Gdansk, S-E Baltic
1649 Sea), *Marine Chemistry*, 186, 211–220, <https://doi.org/10.1016/j.marchem.2016.10.002>, 2016.
- 1650 Łukawska-Matuszewska, K. and Dwornik, M.: Early diagenesis in anoxic sediments of the
1651 Gulf of Gdańsk (southern Baltic Sea): Implications for porewater chemistry and benthic flux
1652 of carbonate alkalinity, *Frontiers in Earth Science*, 13,
1653 <https://doi.org/10.3389/feart.2025.1593031>, 2025.
- 1654 Łukawska-Matuszewska, K., Kielczewska, J., and Bolalek, J.: Factors controlling spatial
1655 distributions and relationships of carbon, nitrogen, phosphorus and sulphur in sediments of
1656 the stratified and eutrophic Gulf of Gdansk, *Continental Shelf Research*, 85, 168–180,
1657 <https://doi.org/10.1016/j.csr.2014.06.010>, 2014.
- 1658 Łukawska-Matuszewska, K., Broclawik, O., Brodecka-Goluch, A., Rzepa, G., Manecki, M.,
1659 and Bolalek, J.: Biogeochemical and mineralogical effects of Fe-P-S dynamics in sediments
1660 of continental shelf sea: Impact of salinity, oxygen conditions, and catchment area
1661 characteristics, *Science of The Total Environment*, 807, 151035,
1662 <https://doi.org/10.1016/j.scitotenv.2021.151035>, 2022.
- 1663 Łukawska-Matuszewska, K., Brodecka-Goluch, A., Czachor, A., and Rios-Quintero, R.: Gas
1664 bubble release areas as new potential hot spots for water column enrichment with nutrients in
1665 eutrophicated sea, *Marine Environmental Research*, 205, 106981,
1666 <https://doi.org/10.1016/j.marenvres.2025.106981>, 2025.
- 1667 Lundsten, E., Paull, C. K., Gwiazda, R., Dobbs, S., Caress, D. W., Kuhnz, L. A., Walton, M.,
1668 Nieminski, N., McGann, M., Lorensen, T., Cochrane, G., and Addison, J.: Pockmarks
1669 offshore Big Sur, California provide evidence for recurrent, regional, and unconfined
1670 sediment gravity flows, *Journal of Geophysical Research: Earth Surface*, 129,
1671 e2023JF007374, <https://doi.org/10.1029/2023JF007374>, 2024.
- 1672 Lynes, M. M., Jay, Z. J., Kohtz, A. J., and Hatzenpichler, R.: Methylo-trophic methanogenesis
1673 in the Archaeoglobi revealed by cultivation of *Ca. Methanoglobus hypatiae* from a
1674 Yellowstone hot spring, *The ISME Journal*, 18, wrae026,
1675 <https://doi.org/10.1093/ismejo/wrae026>, 2024.
- 1676 Maeder, D. L., Anderson, I., Brettin, T. S., Bruce, D. C., Gilna, P., Han, C. S., Lapidus, A.,
1677 Metcalf, W. W., Saunders, E., Tapia, R., and Sowers, K. R.: The *Methanosarcina barkeri*
1678 genome: comparative analysis with *Methanosarcina acetivorans* and *Methanosarcina mazei*

- 1679 reveals extensive rearrangement within methanosarcinal genomes, *Journal of Bacteriology*,
1680 188, 7922–7931, <https://doi.org/10.1128/JB.00810-06>, 2006.
- 1681 Majewski, P. and Klusek, Z.: Expressions of shallow gas in the Gdansk Basin, *Zeszyty*
1682 *Naukowe Akademii Marynarki Wojennej*, 52, 61–71, 2011.
- 1683 Martens-Habbena, W. and Qin, W.: Archaeal nitrification without oxygen, *Science*, 375, 27–
1684 28, <https://doi.org/10.1126/science.abn0373>, 2022.
- 1685 Moore, W. S.: The subterranean estuary: a reaction zone of ground water and sea water,
1686 *Marine Chemistry*, 65, 111–125, [https://doi.org/10.1016/S0304-4203\(99\)00014-6](https://doi.org/10.1016/S0304-4203(99)00014-6), 1999.
- 1687 Moore, W. S.: The effect of submarine groundwater discharge on the ocean, *Annual Review*
1688 *of Marine Science*, 2, 59–88, <https://doi.org/10.1146/annurev-marine-120308-081019>, 2010.
- 1689 Niemann, H. and Elvert, M.: Diagnostic lipid biomarker and stable carbon isotope signatures
1690 of microbial communities mediating the anaerobic oxidation of methane with sulphate,
1691 *Organic Geochemistry*, 39, 1668–1677, <https://doi.org/10.1016/j.orggeochem.2007.11.003>,
1692 2008.
- 1693 O'Reilly, S. S., Jordan, S. F., Monteys, X., Simpson, A. J., Allen, C. C. R., Szpak, M. T.,
1694 Murphy, B. T., McCarron, S. G., Soong, R., Wu, B., Jenne, A., Grey, A., and Kelleher, B. P.:
1695 Production of methane and gaseous compounds by surface microbial activity in a small
1696 pockmark field, Dunmanus Bay, Ireland, *Estuarine, Coastal and Shelf Science*, 255, 107340,
1697 <https://doi.org/10.1016/j.ecss.2021.107340>, 2021.
- 1698 Palarea-Albaladejo, J. and Martín-Fernández, J. A.: zCompositions — R package for
1699 multivariate imputation of left-censored data under a compositional approach, *Chemometrics*
1700 *and Intelligent Laboratory Systems*, 143, 85–96,
1701 <https://doi.org/10.1016/j.chemolab.2015.02.019>, 2015.
- 1702 Pancost, R. D., Hopmans, E. C., and Sinninghe Damsté, J. S.: Archaeal lipids in
1703 Mediterranean cold seeps: molecular proxies for anaerobic methane oxidation, *Geochimica et*
1704 *Cosmochimica Acta*, 65, 1611–1627, [https://doi.org/10.1016/S0016-7037\(00\)00562-7](https://doi.org/10.1016/S0016-7037(00)00562-7), 2001.
- 1705 Parsons, T. R., Maita, Y., and Lalli, C. M.: *A Manual of Chemical & Biological Methods for*
1706 *Seawater Analysis*, Pergamon Press, 188 pp., 1984.
- 1707 Peterse, F., Kim, J.-H., Schouten, S., Kristensen, D. K., Koç, N., and Sinninghe Damsté, J. S.:
1708 Constraints on the application of the MBT/CBT palaeothermometer at high latitude
1709 environments (Svalbard, Norway), *Organic Geochemistry*, 40, 692–699,
1710 <https://doi.org/10.1016/j.orggeochem.2009.03.004>, 2009.
- 1711 Petrick, B., Reuning, L., and Martínez-García, A.: Distribution of glycerol dialkyl glycerol
1712 tetraethers (GDGTs) in microbial mats from Holocene and Miocene sabkha sediments,
1713 *Frontiers in Earth Science*, 7, <https://doi.org/10.3389/feart.2019.00310>, 2019.
- 1714 Piekarek-Jankowska, H.: Hydrochemical effects of submarine groundwater discharge to the
1715 Puck Bay [Southern Baltic Sea, Poland], *Geographia Polonica*, 67, 103–119, 1996.
- 1716 Pimenov, N. V., Ulyanova, M. O., Kanapatsky, T. A., Veslopolova, E. F., Sigalevich, P. A.,
1717 and Sivkov, V. V.: Microbially mediated methane and sulfur cycling in pockmark sediments

- 1718 of the Gdansk Basin, Baltic Sea, *Geo-Marine Letters*, 30, 439–448,
1719 <https://doi.org/10.1007/s00367-010-0200-4>, 2010.
- 1720 Pokorski, J.: Geological section through the lower Paleozoic strata of the Polish part of the
1721 Baltic region, *Geological Quarterly*, 54, 123–130, 2010.
- 1722 Purkamo, L., von Ahn, C. M. E., Jilbert, T., Muniruzzaman, M., Bange, H. W., Jenner, A.-K.,
1723 Böttcher, M. E., and Virtasalo, J. J.: Impact of submarine groundwater discharge on
1724 biogeochemistry and microbial communities in pockmarks, *Geochimica et Cosmochimica*
1725 *Acta*, 334, 14–44, <https://doi.org/10.1016/j.gca.2022.06.040>, 2022.
- 1726 Quast, C., Pruesse, E., Yilmaz, P., Gerken, J., Schweer, T., Yarza, P., Peplies, J., and
1727 Glöckner, F. O.: The SILVA ribosomal RNA gene database project: improved data processing
1728 and web-based tools, *Nucleic Acids Research*, 41, D590–D596,
1729 <https://doi.org/10.1093/nar/gks1219>, 2013.
- 1730 Quinn, T. P., Erb, I., Gloor, G., Notredame, C., Richardson, M. F., and Crowley, T. M.: A
1731 field guide for the compositional analysis of any-omics data, *GigaScience*, 8, giz107,
1732 <https://doi.org/10.1093/gigascience/giz107>, 2019.
- 1733 R Core Team: R: A language and environment for statistical computing. R Foundation for
1734 Statistical Computing, 2023.
- 1735 Reeburgh, W. S.: Oceanic methane biogeochemistry, *Chemical Reviews*, 107, 486–513,
1736 <https://doi.org/10.1021/cr050362v>, 2007.
- 1737 Rinke, C., Chuvochina, M., Mussig, A. J., Chaumeil, P.-A., Davin, A. A., Waite, D. W.,
1738 Whitman, W. B., Parks, D. H., and Hugenholtz, P.: A standardized archaeal taxonomy for the
1739 Genome Taxonomy Database, *Nature Microbiology*, 6, 946–959,
1740 <https://doi.org/10.1038/s41564-021-00918-8>, 2021.
- 1741 Roberts, H. H. and Aharon, P.: Hydrocarbon-derived carbonate buildups of the northern Gulf
1742 of Mexico continental slope: A review of submersible investigations, *Geo-Marine Letters*, 14,
1743 135–148, <https://doi.org/10.1007/BF01203725>, 1994.
- 1744 Rogers, D. R. and Casciotti, K. L.: Abundance and diversity of archaeal ammonia oxidizers in
1745 a coastal groundwater system, *Applied and Environmental Microbiology*, 76, 7938–7948,
1746 <https://doi.org/10.1128/AEM.02056-09>, 2010.
- 1747 Rossel, P. E., Lipp, J. S., Fredricks, H. F., Arnds, J., Boetius, A., Elvert, M., and Hinrichs, K.-
1748 U.: Intact polar lipids of anaerobic methanotrophic archaea and associated bacteria, *Organic*
1749 *Geochemistry*, 39, 992–999, <https://doi.org/10.1016/j.orggeochem.2008.02.021>, 2008.
- 1750 Ruiz-González, C., Rodellas, V., and Garcia-Orellana, J.: The microbial dimension of
1751 submarine groundwater discharge: current challenges and future directions, *FEMS*
1752 *Microbiology Reviews*, 45, fuab010, <https://doi.org/10.1093/femsre/fuab010>, 2021.
- 1753 Rzepa, G., Borkowski, A., Manecki, M., Brodecka-Goluch, A., Łukawska-Matuszewska, K.,
1754 Kania, J., Błachowski, A., and De Mey-Śnieżyńska, I.: The effect of freshwater discharge on
1755 the microbialinduced precipitation of minerals in a Baltic Sea bottom pockmark, *Oceanologia*,
1756 in press, 2026.

- 1757 Santoro, A. E., Francis, C. A., De Siewes, N. R., and Boehm, A. B.: Shifts in the relative
1758 abundance of ammonia-oxidizing bacteria and archaea across physicochemical gradients in a
1759 subterranean estuary, *Environmental Microbiology*, 10, 1068–1079,
1760 <https://doi.org/10.1111/j.1462-2920.2007.01547.x>, 2008.
- 1761 Schlüter, M., Sauter, E. J., Andersen, C. E., Dahlgard, H., and Dando, P. R.: Spatial
1762 distribution and budget for submarine groundwater discharge in Eckernförde Bay (Western
1763 Baltic Sea), *Limnology and Oceanography*, 49, 157–167,
1764 <https://doi.org/10.4319/lo.2004.49.1.0157>, 2004.
- 1765 Schmale, O., Schneider von Deimling, J., Gülzow, W., Nausch, G., Waniek, J. J., and Rehder,
1766 G.: Distribution of methane in the water column of the Baltic Sea, *Geophysical Research*
1767 *Letters*, 37, <https://doi.org/10.1029/2010GL043115>, 2010.
- 1768 Schmuck, E. A. and Paull, C. K.: Evidence for gas accumulation associated with diapirism
1769 and gas hydrates at the head of the Cape Fear Slide, *Geo-Marine Letters*, 13, 145–152,
1770 <https://doi.org/10.1007/BF01593187>, 1993.
- 1771 Schouten, S., Hopmans, E. C., Schefuß, E., and Sinninghe Damsté, J. S.: Distributional
1772 variations in marine crenarchaeotal membrane lipids: a new tool for reconstructing ancient sea
1773 water temperatures?, *Earth and Planetary Science Letters*, 204, 265–274,
1774 [https://doi.org/10.1016/S0012-821X\(02\)00979-2](https://doi.org/10.1016/S0012-821X(02)00979-2), 2002.
- 1775 Schouten, S., Hopmans, E. C., and Sinninghe Damsté, J. S.: The organic geochemistry of
1776 glycerol dialkyl glycerol tetraether lipids: A review, *Organic Geochemistry*, 54, 19–61,
1777 <https://doi.org/10.1016/j.orggeochem.2012.09.006>, 2013.
- 1778 Shaw, J., Courtney, R. C., and Currie, J. R.: Marine geology of St. George’s Bay,
1779 Newfoundland, as interpreted from multibeam bathymetry and back-scatter data, *Geo-Marine*
1780 *Letters*, 17, 188–194, <https://doi.org/10.1007/s003670050025>, 1997.
- 1781 Sinninghe Damsté, J. S., Schouten, S., Hopmans, E. C., Duin, A. C. T. van, and Geenevasen,
1782 J. A. J.: Crenarchaeol, *Journal of Lipid Research*, 43, 1641–1651,
1783 <https://doi.org/10.1194/jlr.M200148-JLR200>, 2002.
- 1784 Sinninghe Damsté, J. S., Warden, L. A., Berg, C., Jürgens, K., and Moros, M.: Evaluation of
1785 the distributions of hydroxylated glycerol dibiphytanyl glycerol tetraethers (GDGTs) in
1786 Holocene Baltic Sea sediments for reconstruction of sea surface temperature: the effect of
1787 changing salinity, *Climate of the Past*, 18, 2271–2288, [https://doi.org/10.5194/cp-18-2271-](https://doi.org/10.5194/cp-18-2271-2022)
1788 2022, 2022.
- 1789 Słowakiewicz, M., Whitaker, F., Thomas, L., Tucker, M. E., Zheng, Y., Gedl, P., and Pancost,
1790 R. D.: Biogeochemistry of intertidal microbial mats from Qatar: New insights from organic
1791 matter characterisation, *Organic Geochemistry*, 102, 14–29,
1792 <https://doi.org/10.1016/j.orggeochem.2016.09.006>, 2016.
- 1793 Sowers, K. R., Boone, J. E., and Gunsalus, R. P.: Disaggregation of *Methanosarcina* spp. and
1794 growth as single cells at elevated osmolarity, *Applied and Environmental Microbiology*, 59,
1795 3832–3839, <https://doi.org/10.1128/aem.59.11.3832-3839.1993>, 1993.
- 1796 Stadnitskaia, A., Muyzer, G., Abbas, B., Coolen, M. J. L., Hopmans, E. C., Baas, M., van
1797 Weering, T. C. E., Ivanov, M. K., Poludetkina, E., and Sinninghe Damsté, J. S.: Biomarker

- 1798 and 16S rDNA evidence for anaerobic oxidation of methane and related carbonate
 1799 precipitation in deep-sea mud volcanoes of the Sorokin Trough, Black Sea, *Marine Geology*,
 1800 217, 67–96, <https://doi.org/10.1016/j.margeo.2005.02.023>, 2005.
- 1801 Szczepańska, T. and Uścińowicz, S.: Atlas geochemiczny południowego Bałtyku, Państwowy
 1802 Instytut Geologiczny, Warszawa, 1–55 pp., 1994.
- 1803 Szymczak-Żyła, M. and Lubecki, L.: Biogenic and anthropogenic sources of sedimentary
 1804 organic matter in marine coastal areas: A multi-proxy approach based on bulk and molecular
 1805 markers, *Marine Chemistry*, 239, 104069, <https://doi.org/10.1016/j.marchem.2021.104069>,
 1806 2022.
- 1807 Szymczycha, B., Kroeger, K. D., and Pempkowiak, J.: Significance of groundwater discharge
 1808 along the coast of Poland as a source of dissolved metals to the southern Baltic Sea, *Marine*
 1809 *Pollution Bulletin*, 109, 151–162, <https://doi.org/10.1016/j.marpolbul.2016.06.008>, 2016.
- 1810 Szymczycha, B., Kłostowska, Ż., Kuliński, K., Winogradow, A., Jakacki, J., Klusek, Z.,
 1811 Grabowski, M., Brodecka-Goluch, A., Graca, B., Stokowski, M., Koziorowska, K., and Rak,
 1812 D.: Deep submarine groundwater discharge indicated by pore water chloride anomalies in the
 1813 Gulf of Gdańsk, southern Baltic Sea, *E3S Web of Conferences*, 54, 00035,
 1814 <https://doi.org/10.1051/e3sconf/20185400035>, 2018.
- 1815 Taniguchi, M., Dulai, H., Burnett, K. M., Santos, I. R., Sugimoto, R., Stieglitz, T., Kim, G.,
 1816 Moosdorf, N., and Burnett, W. C.: Submarine groundwater discharge: updates on its
 1817 measurement techniques, geophysical drivers, magnitudes, and effects, *Frontiers in*
 1818 *Environmental Science*, 7, <https://doi.org/10.3389/fenvs.2019.00141>, 2019.
- 1819 Taylor, M. H., Dillon, W. P., and Pecher, I. A.: Trapping and migration of methane associated
 1820 with the gas hydrate stability zone at the Blake Ridge Diapir: new insights from seismic data,
 1821 *Marine Geology*, 164, 79–89, [https://doi.org/10.1016/S0025-3227\(99\)00128-0](https://doi.org/10.1016/S0025-3227(99)00128-0), 2000.
- 1822 Treude, T., Niggemann, J., Kallmeyer, J., Wintersteller, P., Schubert, C. J., Boetius, A., and
 1823 Jørgensen, B. B.: Anaerobic oxidation of methane and sulfate reduction along the Chilean
 1824 continental margin, *Geochimica et Cosmochimica Acta*, 69, 2767–2779,
 1825 <https://doi.org/10.1016/j.gca.2005.01.002>, 2005.
- 1826 Uścińowicz, S. (Ed.): *Geochemistry of Baltic Sea surface sediments*, Polish Geological
 1827 Institute–National Research Institute, Warsaw, 356 pp., 2011.
- 1828 Vaksmaa, A., Guerrero-Cruz, S., van Alen, T. A., Cremers, G., Ettwig, K. F., Lüke, C., and
 1829 Jetten, M. S. M.: Enrichment of anaerobic nitrate-dependent methanotrophic ‘*Candidatus*
 1830 *Methanoperedens nitroreducens*’ archaea from an Italian paddy field soil, *Appl Microbiol*
 1831 *Biotechnol*, 101, 7075–7084, <https://doi.org/10.1007/s00253-017-8416-0>, 2017.
- 1832 Varma, D., Hopmans, E. C., van Kemenade, Z. R., Kusch, S., Berg, S., Bale, N. J., Sangiorgi,
 1833 F., Reichart, G.-J., Sinninghe Damsté, J. S., and Schouten, S.: Evaluating isoprenoidal
 1834 hydroxylated GDGT-based temperature proxies in surface sediments from the global ocean,
 1835 *Geochimica et Cosmochimica Acta*, 370, 113–127, <https://doi.org/10.1016/j.gca.2023.12.019>,
 1836 2024.

- 1837 Virtasalo, J. J., Schröder, J. F., Luoma, S., Majaniemi, J., Mursu, J., and Scholten, J.:
 1838 Submarine groundwater discharge site in the First Salpausselkä ice-marginal formation, south
 1839 Finland, *Solid Earth*, 10, 405–423, <https://doi.org/10.5194/se-10-405-2019>, 2019.
- 1840 Wakeham, S. G., Lewis, C. M., Hopmans, E. C., Schouten, S., and Sinninghe Damsté, J. S.:
 1841 Archaea mediate anaerobic oxidation of methane in deep euxinic waters of the Black Sea,
 1842 *Geochimica et Cosmochimica Acta*, 67, 1359–1374, [https://doi.org/10.1016/S0016-](https://doi.org/10.1016/S0016-7037(02)01220-6)
 1843 [7037\(02\)01220-6](https://doi.org/10.1016/S0016-7037(02)01220-6), 2003.
- 1844 Waters, E., Hohn, M. J., Ahel, I., Graham, D. E., Adams, M. D., Barnstead, M., Beeson, K.
 1845 Y., Bibbs, L., Bolanos, R., Keller, M., Kretz, K., Lin, X., Mathur, E., Ni, J., Podar, M.,
 1846 Richardson, T., Sutton, G. G., Simon, M., Söll, D., Stetter, K. O., Short, J. M., and
 1847 Noordewier, M.: The genome of *Nanoarchaeum equitans*: Insights into early archaeal
 1848 evolution and derived parasitism, *Proceedings of the National Academy of Sciences*, 100,
 1849 12984–12988, <https://doi.org/10.1073/pnas.1735403100>, 2003.
- 1850 Weijers, J. W. H., Schouten, S., Hopmans, E. C., Geenevasen, J. A. J., David, O. R. P.,
 1851 Coleman, J. M., Pancost, R. D., and Sinninghe Damsté, J. S.: Membrane lipids of mesophilic
 1852 anaerobic bacteria thriving in peats have typical archaeal traits, *Environmental Microbiology*,
 1853 8, 648–657, <https://doi.org/10.1111/j.1462-2920.2005.00941.x>, 2006.
- 1854 Weijers, J. W. H., Lim, K. L. H., Aquilina, A., Sinninghe Damsté, J. S., and Pancost, R. D.:
 1855 Biogeochemical controls on glycerol dialkyl glycerol tetraether lipid distributions in
 1856 sediments characterized by diffusive methane flux, *Geochemistry, Geophysics, Geosystems*,
 1857 12, 1–15, <https://doi.org/10.1029/2011GC003724>, 2011.
- 1858 Welte, C., Kröninger, L., and Deppenmeier, U.: Experimental evidence of an acetate
 1859 transporter protein and characterization of acetate activation in aceticlastic methanogenesis of
 1860 *Methanosarcina mazei*, *FEMS Microbiology Letters*, 359, 147–153,
 1861 <https://doi.org/10.1111/1574-6968.12550>, 2014.
- 1862 Werner, F.: Depressions in mud sediments (Eckernförde Bay, Baltic Sea), related to sub-
 1863 bottom and currents, *Meyniana*, 30, 99–104, 1978.
- 1864 Wever, Th. F., Abegg, F., Fiedler, H. M., Fechner, G., and Stender, I. H.: Shallow gas in the
 1865 muddy sediments of Eckernförde Bay, Germany, *Continental Shelf Research*, 18, 1715–1739,
 1866 [https://doi.org/10.1016/S0278-4343\(98\)00055-7](https://doi.org/10.1016/S0278-4343(98)00055-7), 1998.
- 1867 Whiticar, M. J.: Diagenetic relationships of methanogenesis, nutrients, acoustic turbidity,
 1868 pockmarks and freshwater seepages in Eckernförde Bay, *Marine Geology*, 182, 29–53,
 1869 [https://doi.org/10.1016/S0025-3227\(01\)00227-4](https://doi.org/10.1016/S0025-3227(01)00227-4), 2002.
- 1870 Whiticar, M. J. and Werner, F.: Pockmarks: Submarine vents of natural gas or freshwater
 1871 seeps?, *Geo-Marine Letters*, 1, 193–199, <https://doi.org/10.1007/BF02462433>, 1981.
- 1872 Wickham, H.: *ggplot2: Elegant Graphics for Data Analysis*, Springer International Publishing,
 1873 260 pp., 2016.
- 1874 Wilson, S. J., Song, B., Anderson, I. C., and Tobias, C. R.: Nitrification in a subterranean
 1875 estuary: An ex situ and in situ method comparison determines nitrate is available for
 1876 discharge, *Journal of Geophysical Research: Biogeosciences*, 129, e2023JG007876,
 1877 <https://doi.org/10.1029/2023JG007876>, 2024.

- 1878 Wittenborn, A. K., Bauersachs, T., Hassenrück, C., Käding, K., Wäge-Recchioni, J., Jürgens,
1879 K., Arz, H. W., and Kaiser, J.: Nitrosopumilus as main source of isoprenoid glycerol dialkyl
1880 glycerol tetraether lipids in the central Baltic Sea, *Frontiers in Microbiology*, 14,
1881 <https://doi.org/10.3389/fmicb.2023.1216130>, 2023.
- 1882 Wood, D. E., Lu, J., and Langmead, B.: Improved metagenomic analysis with Kraken 2,
1883 *Genome Biology*, 20, 257, <https://doi.org/10.1186/s13059-019-1891-0>, 2019.
- 1884 Yi, X., Brandt, K. K., Xue, S., Peng, J., Wang, Y., Li, M., Deng, Y., and Duan, G.: Niche
1885 differentiation and biogeography of Bathyarchaeia in paddy soil ecosystems: a case study in
1886 eastern China, *Environmental Microbiome*, 19, 13, [https://doi.org/10.1186/s40793-024-](https://doi.org/10.1186/s40793-024-00555-8)
1887 [00555-8](https://doi.org/10.1186/s40793-024-00555-8), 2024.
- 1888 Yu, T., Fu, L., Wang, Y., Dong, Y., Chen, Y., Wegener, G., Cheng, L., and Wang, F.:
1889 Thermophilic Hadarchaeota grow on long-chain alkanes in syntrophy with methanogens,
1890 *Nature Communications*, 15, 6560, <https://doi.org/10.1038/s41467-024-50883-z>, 2024.
- 1891 Zehnder, A. J. B. and Brock, T. D.: Anaerobic methane oxidation: occurrence and ecology,
1892 *Applied and Environmental Microbiology*, 39, 194–204,
1893 <https://doi.org/10.1128/aem.39.1.194-204.1980>, 1980.
- 1894 Zell, C., Kim, J.-H., Hollander, D., Lorenzoni, L., Baker, P., Silva, C. G., Nittrouer, C., and
1895 Sinninghe Damsté, J. S.: Sources and distributions of branched and isoprenoid tetraether
1896 lipids on the Amazon shelf and fan: Implications for the use of GDGT-based proxies in
1897 marine sediments, *Geochimica et Cosmochimica Acta*, 139, 293–312,
1898 <https://doi.org/10.1016/j.gca.2014.04.038>, 2014.
- 1899 Zeng, Z., Chen, H., Yang, H., Chen, Y., Yang, W., Feng, X., Pei, H., and Welander, P. V.:
1900 Identification of a protein responsible for the synthesis of archaeal membrane-spanning
1901 GDGT lipids, *Nature Communications*, 13, 1545, [https://doi.org/10.1038/s41467-022-29264-](https://doi.org/10.1038/s41467-022-29264-x)
1902 [x](https://doi.org/10.1038/s41467-022-29264-x), 2022.
- 1903 Zhang, Y. G., Zhang, C. L., Liu, X.-L., Li, L., Hinrichs, K.-U., and Noakes, J. E.: Methane
1904 Index: A tetraether archaeal lipid biomarker indicator for detecting the instability of marine
1905 gas hydrates, *Earth and Planetary Science Letters*, 307, 525–534,
1906 <https://doi.org/10.1016/j.epsl.2011.05.031>, 2011.
- 1907 Zhang, Z., Shan, H., Feng, X., Jia, Z., Jiang, L., Wang, S., and Zhu, C.: Review of research
1908 progress on the impact of submarine groundwater discharge on pockmark formation and
1909 evolution, *Journal of Marine Science and Engineering*, 13, 1070,
1910 <https://doi.org/10.3390/jmse13061070>, 2025.
- 1911 Zhou, Z., Pan, J., Wang, F., Gu, J.-D., and Li, M.: Bathyarchaeota: globally distributed
1912 metabolic generalists in anoxic environments, *FEMS Microbiology Reviews*, 42, 639–655,
1913 <https://doi.org/10.1093/femsre/fuy023>, 2018.
- 1914 Zinke, L. A., Glombitza, C., Bird, J. T., Røy, H., Jørgensen, B. B., Lloyd, K. G., Amend, J. P.,
1915 and Reese, B. K.: Microbial organic matter degradation potential in Baltic Sea sediments is
1916 influenced by depositional conditions and in situ geochemistry, *Applied and Environmental*
1917 *Microbiology*, 85, e02164-18, <https://doi.org/10.1128/AEM.02164-18>, 2019.
- 1918